SLAC-PUB-5907
September 1992
(A)

LONGITUDINAL ELECTROMAGNETIC FIELDS IN AN APERIODIC STRUCTURE*

S. A. Heifets, S. A. Kheifets
Stanford Linear Accelerator Center
Stanford University, Stanford, CA 94309

ABSTRACT

The propagation of the electromagnetic wave in an aperiodic disk-loaded accelerating section have been studied using field-matching technique. A matrix formalism similar to one of the scattering theory is applied. The method developed allows study of an arbitrarily large number of irises and radial space harmonics. Reflection and transmission coefficients of the structure, its wave and coupling impedances, beam loading, and other characteristics have been calculated as a function of the wave frequency. The modifications of the reflection coefficient by couplers has also been studied. Two examples are given: one is a constant impedance structure consisting of 30 cells; the other is a detuned accelerating structure designed at SLAC for the Next Linear Collider consisting of over two hundred cells.

Submitted to *IEEE Transactions on Microwave Theory and Techniques*

*Work supported by the Department of Energy, contract DE-AC03-76SF00515.

I. INTRODUCTION

The next generation of linear colliders will most probably utilize disk-loaded structures only slightly more complicated than the accelerating sections of the SLAC Linear Collider (SLC). The main difference being the higher frequency of the accelerating field (11.424 GHz), to facilitate a higher accelerating gradient, and a Gaussian distribution of the dipole mode frequencies of individual cells [1-4] (*detuned structure*) with the aim of suppressing the multibunch beam breakup. For example, the prototype accelerating section designed at SLAC for the Next Linear Collider (NLC) is, basically, a cylindrical beam pipe loaded by over 200 irises, producing thus a chain of coupled RF cavities. Each cell consists of a cavity with a gap length g and an adjacent iris of the thickness l. In each cell the pair of radii of a cavity b and an iris a (see Table 1) are chosen to produce the same frequency of the fundamental accelerating field. The frequencies of the dipole modes vary from cell to cell, minimizing the strengths of the long range transverse wakefield.

Until now, the design of an aperiodic accelerator section was based on the assumption that the parameters of the section at a given point of the structure are close to the corresponding parameters of the cell located there and that they vary only slowly along the structure. In such an approach one essentially assumes the local field in the aperiodic structure to be that of a corresponding periodic structure, with the local dimensions of the aperiodic structure. There are several known reliable methods and computer codes [5-7] for calculations of the infinitely periodic structures. However, there always arises the question of how good is this approximation for the travelling wave structures. The important features arising from the structure ends should also be carefully taken into account. This is why it is desirable to develop a straightforward method to calculate the electromagnetic (EM) fields excited in the travelling wave structures.

It is worth mentioning the previous studies [8-10] of the transverse wakefields excited in a detuned structure. They are based on an equivalent circuit model. However, any such an approach can never include all the characteristics of the real structure. Here again, reliable methods are needed that do not depend on model considerations.

The aim of the work described here is development of a technique suitable for the study of problems arising in the design of aperiodic RF structures.

Simulations of the EM wave propagation in an aperiodic structure is a challenging problem. The derivation of the exact system of linear algebraic equations for the modal analysis can easily be achieved using the standard field-matching technique. However, the solution of such a system is not trivial, even for a single iris in the pipe [11,12].

A general method for studying the propagation and the excitation of the EM fields in an aperiodic structure with piecewise constant radii is described in this paper. The computer code *PROGON*, based on the developed method, has been written for the numerical calculations. All the results reported here were obtained using this code. The method is based on the field-matching technique (see Sec. 2). The corresponding truncated system of algebraic equations is solved numerically. The formalism employes matrices of relatively small sizes that depend only on the number of cavity modes taken into account. Thus the number of cells is relevant only for the computational time. In one example given here, the method is applied to a detuned SLAC accelerating structure consisting of over 200 cells.

The matrix formalism developed here is similar to that of the scattering theory [13]. It is described in detail in the Appendix to this note. The irises variables are excluded without increasing the matrix size. The convergence of the method does not depend on any special relation [14] between the number of spatial harmonics in the cavities and the irises included in the calculations. It is shown that the

larger those numbers are, the better the approximation to the solution that can be obtained. In addition, such an exclusion of the irises variables may have a future advantage, allowing development of a formalism that can handle more or less arbitrary shapes of irises. This could be done by supplying the program with a subroutine relating one side of an iris to the other.

A particular case of the infinite periodic structure is considered in Sec. 3. The eigenvalue problem is solved in this case to find the dispersion curves and the passbands of the section. The results are in agreement with the existing codes. Notice that for a detuned structure, the concepts of a dispersion curve, phase and group velocity, etc., have limited meaning since all of these parameters change along the section. Nevertheless, when the cell dimensions vary along the section slowly enough, these concepts preserve their local meaning. The formalism developed here is not limited to slow variation of the cell dimensions.

We next study a scattering problem for a monochromatic RF wave in the aperiodic structure (see Sec. 4). The boundary conditions at the ends of the accelerating section follow naturally from the general radiation conditions for the reflected and transmitted travelling waves. The geometry of the end cells (*couplers*) are chosen to suppress the reflection coefficient for the structure in a broad band of frequencies (see Sec. 5). The energy gain by a test particle is found as a function of frequency in Sec. 6.

Next, in Sec. 7, the excitation of the field by a train of point charges is considered. The formalism is extended for this purpose onto the inhomogeneous Maxwell equations. The longitudinal wake function, the corresponding longitudinal coupling impedance of the structure, and the beam loading by a train of bunches are calculated.

The solution found shows its internal consistency. For example, the number and spacing of peaks in the transmission coefficient as a function of the

frequency agrees with the estimate that is based on the calculated width of the passband; the frequency at which the wave impedance reaches its maximum coincides to an accuracy better than 10^{-4}, with the frequency that corresponds to the phase velocity of the wave equal to the velocity of light; and so on.

The extension of the method onto the transverse wakefields should be straightforward, and is intended for future work.

2. FIELD MATCHING

To make our task as simple as possible, consideration here is restricted to the case of the axially symmetric accelerating field ($m = 0$). The geometry of the structure and the coordinate system chosen are shown in Fig. 1. In what follows, we consider an ultrarelativistic case $v \to c$, and the lossless structures with infinite wall conductivity $\sigma \to \infty$. Throughout the note, we deal with the Fourier harmonics of the EM fields, and of the current density corresponding to a circular frequency $\omega = 2\pi f$.

Consider a train of pointlike bunches with the charge eN_B, each moving along the axis of the section at the speed of light c. Let the mth bunch be positioned at time $t = 0$ at $z = s_m$. The longitudinal component of the current density of such a train is

$$j(r,\phi,z,t) \;=\; eN_B c\,[\delta(r)/r] \quad \delta(\phi)\,\sum\nolimits_m \delta(z - ct - s_m)\,. \tag{2.1}$$

Its Fourier harmonic is

$$\begin{aligned} j(r,\phi,z,k) \;&=\; \int_{-\infty}^{\infty} dt\; j(r,\phi,z,t)\;\exp\{i\omega t\} \\ &=\; eN_B\,[\delta(r)/r] \quad \delta(\phi)\,\sum\nolimits_m \exp\{ik(z - s_m)\}\;, \end{aligned} \tag{2.2}$$

where $k = \omega/c$.

The following convention for numbering the cavities and irises is used. The cells in the array are numbered by superscript N, $N = 1, 2, \ldots N_c$, the iris preceding the Nth cavity having the same number N. The structure starts with a cavity ($N = 1$, actually extending to $-\infty$), that is followed by an iris $N = 2$. Similarly, the section ends with an iris $N = N_c$ and a cavity $N = N_c$ (that actually extends to $+\infty$).

For axially symmetric problems, of a possible two sets of the solution of the Maxwell equations, only TM monopole ($m = 0$) modes are essential and sufficient to describe the longitudinal field dynamics.

Inside a cylindrical pipe with constant radius, all the nonzero components E_r, E_z and H_ϕ of the TM type of the EM field can be represented by a sum of a particular solution driven by an external current density $j(r, \phi, z, k)$ and a general solution of the homogeneous equations. The latter part can be represented as an expansion into a series of cylindrical waves with unknown complex amplitudes. For example, for the region inside the Nth cavity of the radius b^N, the longitudinal Fourier harmonic of the electric field E_z on the frequency $f = kc/2\pi$ can be represented as

$$E_z^N(r, z, k) = \sum_{n=1}^{\infty} (\nu_n/b^N)^2 \, J_0(\nu_n r/b^N) \; x_n^N(z) \, . \tag{2.3}$$

Similarly, for the Nth iris with the radius a^N,

$$E_z^N(r, z, k) = \sum_{n=1}^{\infty} (\nu_n/a^N)^2 \, J_0(\nu_n r/a^N) \; \xi_n^N(z) \, . \tag{2.4}$$

Here z is the distance from the left end of a cavity or an iris. The expansion of all the essential field components can be found in the Appendix. Each of the

propagation functions, $x_n^N(z)$ or $\xi_n^N(z)$, is a superposition of two waves travelling in $+z$ (forward wave) or in $-z$ (backward wave) directions:

$$x_n^N(z) = \overrightarrow{C}_n^N \exp\{i\lambda_n^N z\} + \overleftarrow{C}_n^N \exp\{-i\lambda_n^N z\}\,, \qquad 0 < z < g^N \qquad (2.5)\,,$$

$$\xi_n^N(z) = \overrightarrow{D}_n^N \exp\{i\mu_n^N z\} + \overleftarrow{D}_n^N \exp\{-i\mu_n^N z\}\,, \qquad 0 < z < l^N \qquad (2.6)\,,$$

where the propagation constants are

$$\lambda_n^N = \sqrt{k^2 - (\nu_n/b^N)^2}\,, \qquad (2.7)$$

$$\mu_n^N = \sqrt{k^2 - (\nu_n/a^N)^2}\,. \qquad (2.8)$$

In the array of coupled cavities, each eigenmode of a cavity generates a passband of the array. If the coupling between cavities is weak enough, the passbands do not overlap.

Subsequent derivations essentially depend on the choice of the wave number k. Consider, for example, the most interesting case of the frequencies within the first passband. The first spatial mode in each cavity (corresponding to $n = 1$) is the only truly travelling mode, since its propagation constant λ_1^N is real. All the other modes ($n > 1$) are evanescent waves with pure imaginary propagating constants. For the irises, all the propagation constants μ_n^N, including the first one, are imaginary. For $|k| < \nu/a^N, Im(k) > 0$

$$\mu_n^N(k) = i\sqrt{(\nu_n/a^N)^2 - k^2}\,. \qquad (2.9)$$

Most of the paper deals with this case.

To satisfy the boundary and continuity conditions, it is sufficient to consider two of the three field components—either E_r, H_ϕ or E_r, E_z. We choose here the

pair of components E_z and E_r. Each radial mode, Eqs. (A.2-5) of the Appendix, satisfies the boundary condition on the cylindrical surfaces $r = a^N$, $0 < z < l^N$ or $r = b^N$, $0 < z < g^N$, respectively. The amplitudes $\overrightarrow{C}_n^N$, $\overleftarrow{C}_n^N$, $\overrightarrow{D}_n^N$ and $\overleftarrow{D}_n^N$ should be chosen in such a way as to satisfy the boundary and continuity conditions on the remaining metal walls of the irises. Consider, for example, the interface between a cavity with radius b, and the subsequent iris with the radius of the aperture a. The continuity conditions on the aperture at $z = g$ are

$$E_z(r, g-0, k) \;=\; E_z(r, g+0, k)\;; \qquad \text{for all } \; 0 < r < a\;, \qquad (2.10)$$

and

$$E_r(r, g-0, k) \;=\; E_r(r, g+0, k)\;\theta(a-r)\;; \qquad \text{for all } \; 0 < r < b\;, \qquad (2.11)$$

where $\theta(x)$ is a step function, $\theta(x) = 1$ for $x > 0$, $\theta(x) = 0$ for $x < 0$.

As one can see, for the considered formalism the cavity gaps g^N, and the radii b^N, the iris thicknesses l^N, and the apperture radii a^N can all be different. For a structure for which all the radii a^N of the openings have the same value a and all the radii b^N of the cavities have another value b, there is the option of matching the fields on the interface $r = a$. However, in the general case of different a^N and b^N, the matching on the interfaces Z=const is much simpler.

From Eqs. (2.10-11), there follows the system of linear algebraic equations for unknown quantities $x_n^N(0)$ and $x_n^{N-1}(g^{N-1})$; i.e., the values of the propagation function at $z = 0$ and $z = g^{N-1}$. This system is derived in the Appendix.

We construct from $x_n^N(0)$ and $x_n^{N-1}(g^{N-1})$ the set of vectors f_i^N, $i = 1, 2, \ldots, 2J^C$, where J^C is the truncation number; i.e., the maximum number of

the spatial cavity modes taken into account. The vector f^N describes the field on the both sides of the Nth iris:

$$f_i^N \equiv x_i^N(0) , \qquad i = 1, \ldots, J^C , \tag{2.12}$$

$$f_{i+J}^N \equiv x_i^{N-1}(g^{N-1}) , \qquad i = 1, \ldots, J^C . \tag{2.13}$$

The vectors f_i^N of the rank $2J^C$ satisfy the system of the recurrence equations

$$A^N f^N = B^N f^{N-1} + F^N f^{N+1} + G^N , \qquad N = 2, 3, \ldots, N_c . \tag{2.14}$$

The recurrence equations of this type is characteristic for any coupled linear chain of elements. In our case the cavities comprise such a coupled chain: the field in each cavity depends on the field in its neighbors on the left- and the right-hand side of it. Matrices A^N, B^N, F^N of the rank $2J^C \times 2J^C$ and vectors G^N of the rank $2J^C$, as well as the method of finding the solution of Eqs. (2.14),. are given in the Appendix.

3. INFINITE PERIODIC STRUCTURE

A particular case of the considered structure is a periodic structure with the period $d = g + l$, consisting of the infinite number of identical cells. Finding the field in such a structure is tantamount to solving the eigenvalue problem.

The equations to be solved in this case are homogeneous equations (2.14), where $G^N \equiv 0$. All the matrices R, Q (see Appendix), A, B, and F are the same, and the superscript N may be omitted. According to the Floque theorem,

the fields in the cavities with numbers $N+1$ and N are the same—apart of the constant complex factor

$$f^{N\pm1}(z) \;=\; \exp\{\pm i\psi\}\; f^{N}(z)\;. \tag{3.1}$$

Hence, the solution has the form $f^N(z) = e^{i\psi}V(z)$, where $V(z)$ is a periodic vector $V(z+d) = V(z)$. Eq. (2.14) then become the following matrix equation:

$$[A(k) - B(k)\;\exp\{-i\psi\}\; - F(k)\;\exp\{i\psi\}]\;V \;=\; 0\;. \tag{3.2}$$

The system of homogeneous Eqs. (3.2) may have a nontrivial solution only if its determinant is equal zero

$$|\,A(k) - B(k)\;\exp\{-i\psi\} - F(k)\;\exp\{i\psi\}\,| \;=\; 0\;. \tag{3.3}$$

The set of solutions of this equation k, ψ that correspond to real values of ψ define the passband of the array. The curve $k(\psi)$ inside the passband is the dispersion curve, and ψ has the meaning of the phase shift per period. The range of the ψ variation is $-\pi < \psi < \pi$.

Consider, for example, a single spatial mode in the cavity. In this case, Eq. (3.3) is reduced to (see the Appendix),

$$\begin{vmatrix} -Q - (\lambda/\tan\beta) & R + \exp\{i\psi\}\,(\lambda/\sin\beta) \\ -R - \exp\{-i\psi\}(\lambda/\sin\beta) & Q + (\lambda/\tan\beta) \end{vmatrix} \;=\; 0\;, \tag{3.4}$$

where $\lambda = \lambda_1$, $\beta = g\lambda_1$, $Q = Q_{11}$ and $R = R_{11}$. All these quantities are functions of k.

Solving in respect to ψ gives the following dispersion equation:

$$\cos\psi \;=\; (Q/R)\;\cos\beta \;+\; \left[(Q^2-R^2-\lambda^2)/2R\right] \quad (\sin\beta/\lambda)\;. \qquad (3.5)$$

For a very thick iris $l \to \infty$, $R \to 0$ and this equation defines the frequencies k_1 of the eigenmodes of an isolated pillbox cavity with attached tubes:

$$\tan\beta(k_1) = -2\lambda Q/(Q^2-\lambda^2)\;. \qquad (3.6)$$

For a finite but small R

$$\sin\beta = -\left[2\lambda Q/\left(Q^2-\lambda^2\right)\right] \quad [\cos\beta - (R/Q)\;\cos\psi] \qquad (3.7)$$

or

$$k^2(\psi) \;=\; k_1^2 - (2\lambda R/gQ)\;\cos\psi\;, \qquad (3.8)$$

where k_1 is the solution of Eq. (3.6).

The dispersion curve $k(\psi)$ is similar to the dispersion curve for the chain of coupled oscillators, with the coupling strength proportional to R. This quantity defines the width of the passband.

The dispersion curves for an infinite periodic array built out of the first, the middle, and the last cells of the detuned 204-cell accelerating section has been calculated using the determinant of the truncated system, Eq. (3.3). The dimensions of all the cavities and irises used in the calculations are listed in Table 1. The first J^C spatial cavity modes and the first J^W spatial iris modes were taken into account. The results of the calculations are shown in Figs. 2–4 as symbols, along with the curves that were obtained with the help of the code *KN7C* [5]. For the considered dimensions, the frequency width of the first passband is of the order of 1 GHz for the first, and of 400 MHz for the last cavity.

The agreement between these two sets of results is quite good for large enough J^C and J^W. Figure 3 represents the dispersion curve that corresponds to the first cavity calculated with $J^W = 50$ and for a number of different truncation numbers, J^C. It demonstrates the convergence of the dispersion curve to a limiting shape with the increase of J_C. In Fig. 4, the independence of the dispersion curve for the first cavity on the J^W for $J^W > 16$ is demonstrated, assuming $J^C = 16$.

Figure 5 is a blowup of the portion of Fig. 3 indicated on it by a dashed rectangle. The dashed straight line corresponds to the phase velocity of the wave equal to that of light $v_{\rm ph} = c$. The phase advance per cell and the frequency of the synchronous wave are defined by the intersection of the curve with the dashed line. For the truncation number, $J^C = 20$ $\psi \simeq 2\pi/3$ and $f \simeq 11.431$ GHz. This frequency is shifted by ≈ 7 MHz from the designed frequency 11.424 GHz. The difference is mostly due to the rounded shape of the iris edge of the designed structure, in comparison to the rectangular shape assumed in the present calculations. Figure 6 gives the dispersion curves of the first two passbands for the 30-cell experimental constant impedance section. The cell dimensions of this section can be found in Table 1.

After the phase shif ψ is found, Eq. (3.2) defines the vector V in each cell, and thus the EM field pattern in the periodic structure.

4. APERIODIC STRUCTURE

We turn now to the problem of finding the travelling EM field in an aperiodic structure. In this and two subsequent sections we will concentrate on the problem of the propagation of a wave with the wave number k arriving from $z = -\infty$. For this purpose, the terms arising from the beam current, i.e., all the terms proportional to N_B, should be dropped. The excitation of the structure by a beam

current is considered in Section 7. We assume also that the frequency of the incident wave lies in the first passband of the section.

The EM fields in a finite length structure depend significantly on the physical conditions on its ends. One can formulate them from the following simple physical considerations. The complex amplitude of the incident fundamental forward-travelling wave entering the structure from the left is arbitrary. Its evanescent modes decay at $Z = -\infty$. Hence, for the first passband, the coefficients $\overrightarrow{C}_n^1$ must be chosen in the following way:

$$\overrightarrow{C}_n^1 = 0 , \qquad n = 2, 3, \ldots . \tag{4.1}$$

Similarly, at the right end of the structure:

$$\overleftarrow{C}_n^{N_c} = 0 , \qquad n = 1, 2, \ldots . \tag{4.2}$$

Conditions in Eqs. (4.1),(4.2) for the amplitudes $\overrightarrow{C}^1$ and $\overleftarrow{C}^{N_c}$ mean that the values of the propagation functions and their derivatives x^1, y^1 at the left end of the section are related to each other in the following way:

$$y_n^1(g^1) = -i\lambda_n^1 x_n^1(g^1) , \qquad n = 2, 3, \ldots, J^C . \tag{4.3}$$

Similarly, at the right end of the section, x^{N_c}, y^{N_c} are related to each other in the following way:

$$y_n^{N_c}(0) = i\lambda_n^{N_c} x_n^{N_c}(0) , \qquad n = 1, 2, \ldots, J^C . \tag{4.4}$$

The amplitude $x_1^1(0)$ remains arbitrary. All the other amplitudes are proportional to it. Hence, it can be considered as the source of the field excitation and moved into the right-hand side of the equations. All these conditions are reflected in the structure of the matrix elements A^N, B^N, F^N and G^N, listed in the Appendix.

The vector f^{N_c+1} can be chosen arbitrary because it does not enter Eq. (A.36), since $F^{N_c} = 0$ [see, Eq. (A.40) of the Appendix]. Hence, one can assume $f^{N_c+1} = 0$. It then follows that matrices $\mathcal{A}^{N_c} = \mathcal{B}^{N_c} = 0$. Using the recurrence Eqs. (A.49–50) and beginning with these values, one finds sequentially all matrices $\mathcal{A}^N, \mathcal{B}^N$, for $N = N_c - 1, \ldots, 1$. Similarly, the vector f^1 does not enter Eq. (A.36), since $B^2 = 0$ [see, Eq. (A.44) of the Appendix]; hence, one can assume $f^1 = 0$. Now using Eqs. (A.48) and the found matrices $\mathcal{A}^N, \mathcal{B}^N$, one finds sequentially all f^N for $N = 2, \ldots, N_c$.

After the vectors f^N (and consequently, the vectors $x_n^N(0)$ and $x_n^N(g^N)$) are found, vectors $y_n^N(0)$ and $y_n^N(g^N)$ can be calculated with the help of Eqs. (A.13) and (A.16), and vectors $\xi_n^N(0)$ and $\xi_n^N(l^N)$ can be calculated with the help of Eqs. (A.14) and (A.15), respectively. Then Eqs. (A.8) and (A.4), and respectively Eqs. (A.9) and (A.7), can be used to find amplitudes $\overrightarrow{C}_n^N$ and $\overleftarrow{C}_n^N$ of the forward and backward waves in the cavities, and $\overrightarrow{D}_n^N$ and $\overleftarrow{D}_n^N$ of the forward and backward waves in the irises. This defines the fields at any point in the structure.

There are several ways to verify that the obtained solution is the correct one. One of them is the trivial back substitution of the found vectors f^N into Eq. (2.14). Numerical solution satisfies this condition to an accuracy better than 10^{-14}. Next, since there is no energy dissipation inside the system, the energy flow through any of its cross sections should be independent of the Z coordinate and the same in all cells.The integral of the z component of the Pointing vector over the cavity cross section S can be expressed in terms of the amplitudes of the forward, $\overrightarrow{C}_n^N$, and backward, $\overleftarrow{C}_n^N$, waves. For a monochromatic wave,

$$E_z^N(r,z,t) = \sum_{n=1}^{n=J^C} (\nu_n/b^N)^2 \, J_0(\nu_n r/b^N) \times \left[\exp\{-i\omega t\} \left(\overrightarrow{C}_n^N \exp\{i\lambda_n^N z\} + \overleftarrow{C}_n^N \exp\{-i\lambda_n^N z\} \right) + \text{c.c.} \right], \tag{4.5}$$

the energy flow is

$$
\begin{aligned}
P(\omega) \;\equiv\; & (c/4\pi) \int dS \; \left[E_r^N(k)\, H_\phi^{N*}(k) + \text{c.c.} \right] \\
= \; & (\omega/2) \left[\nu_1^2 \, J_1^2(\nu_1) \, \lambda_1^N \Big(\mid \overrightarrow{C}_1^{\,N} \mid^2 - \mid \overleftarrow{C}_1^{\,N} \mid^2 \Big) \right. \\
& \left. - \; 2 \sum\nolimits_{n=2}^{n=J^C} \nu_n^2 \, J_1^2(\nu_n) \mid \lambda_n^N \mid \mathrm{Im} \Big(\overrightarrow{C}_n^{\,N} \, \overleftarrow{C}_n^{\,N*} \Big) \right] ,
\end{aligned}
\tag{4.6}
$$

where c.c. and an asterisk denote a complex conjugate value. The obtained solution produces a constant energy flow P throughout the section.

Further, the correct solution should reproduce the boundary and continuity conditions, Eqs. (2.10-11). Figures 7 and 8 illustrate the degree to which these conditions are satisfied. In Fig. 7, the real and imaginary parts of the radial component of the electric field E_r on the surface of one of the irises are plotted as a function of the relative cavity radius r/b. The curves represent the field E_r calculated on both the cavity side and the iris side of the metal wall, $r = a$. The position of iris edge $r = a$ is shown by a vertical dashed line.

Similarly, Fig. 8 represent the real and imaginary parts of the longitudinal component of the electric field E_z along the detuned section versus the cell number. Both examples are obtained with $J^C = 20$ and $J^W = 30$.

5. REFLECTION AND TRANSMISSION COEFFICIENTS

In this Section we consider the most interesting case, when the frequency of the incident wave lies in the first passband of the structure. In other words, there is only one spatial mode with the real propagation constant λ_1^N. In this case, the EM field in the waveguide to the left of the section is defined solely by the propagation function $x_1^1(z)$ and its derivative $y_1^1(z)$ of the first cavity. Indeed, the forward amplitudes $\overrightarrow{C}_n^{\,1} = 0$ for $n > 1$ [see Eq. (4.1)] and, hence, the evanescent

fields do not contribute to the energy flow of the incident wave. All the spatial modes of the reflected (backward) wave with indices $n > 1$ are evanescent, and they decay exponentially for $z < 0$. Hence, the propagating mode $n = 1$ has the following form:

$$x_1^1(z) = \overrightarrow{C}_1^1 \exp\{i\lambda_1^1 z\} + \overleftarrow{C}_1^1 \exp\{-i\lambda_1^1 z\} . \tag{5.1}$$

The reflection coefficient $\mathcal{R}(\omega)$ is defined by the ratio of the complex amplitudes $\overrightarrow{C}_1^1$ and $\overleftarrow{C}_1^1$

$$\mathcal{R}(\omega) = \overleftarrow{C}_1^1(\omega) \Big/ \overrightarrow{C}_1^1(\omega) . \tag{5.2}$$

The absolute value of the square of the reflection coefficient $\mathcal{R}$ is the ratio of the power reflected from the section to the power of the incident RF wave.

Similarly, the energy flow of the transmitted EM field in the waveguide to the right of the section—i.e., for $Z > L \equiv N_c d$—is defined solely by the propagation function $x_1^{N_c}(z)$ and its derivative $y_1^{N_c}(z)$. According to Eq. (4.2), function $x_1^{N_c}(z)$ describes the forward wave only:

$$x_1^{N^c}(z) = \overrightarrow{C}_1^{N_c} \exp\left\{i\lambda_{N_c}^1 (Z - L)\right\} . \tag{5.3}$$

All the spatial modes with $n > 1$ decay exponentially for $Z > L$. Hence, the transmission coefficient $\mathcal{T}(\omega)$ is defined by the ratio

$$\mathcal{T}(\omega) = \sqrt{\lambda_1^{N_c}}\, \overrightarrow{C}_1^{N_c}(\omega) \Big/ \sqrt{\lambda_1^1}\, \overrightarrow{C}_1^1(\omega) . \tag{5.4}$$

The absolute value of the square of the transmission coefficient T is the ratio of the power transmitted through the section to the power of the incident RF wave.

Since the structure is lossless, the two coefficients for any frequency satisfy the relation:

$$|\mathcal{R}(\omega)|^2 + |\mathcal{T}(\omega)|^2 = 1 . \tag{5.5}$$

The variation in behavior of the reflection and transmission coefficients with frequency strongly depends on the matching between the impedance of a structure and the impedances of the adjacent wave guides. The matching is usually achieved by adjusting the parameters of couplers at the end of a section. In the present study, the second and the penultimate cavities of the section are used as the couplers. They were adjusted by varying their three parameters a, b and g, thus maintaining the axial symmetry of the problem. To minimize the reflection coefficient in the vicinity of the designed frequency, we closely follow the SLAC procedure [16] for the couplers adjustment. First, we temporarily introduced field damping in the section. The damping rate was gradually increased, starting from zero at the left (entrance) end and moving to the right (exiting) end of the section. Under these conditions, the dimensions of the left coupler were found by minimizing the reflection coefficient. Then the damping was turned off, and the parameters of the right coupler were optimized in the same way.

The reflection $\mathcal{R}$ and transmission $\mathcal{T}$ coefficients as a function of the frequency of the incident wave are calculated here for two accelerating sections with dimensions [17] that can be found in the accompanying paper [18].

In Fig. 9, the absolute values and the phases of $\mathcal{R}$ and $\mathcal{T}$ are plotted for the 30-cell constant impedance structure for two cases.

A. The case without couplers, curve a.

The resonant character of the coefficients are clearly exhibited. The resonances are spaced at approximately $\Delta f/N_c$, where Δf is the frequency width of the structure passband (≈ 300 MHz for the considered cell geometry, see Fig. 6).

B. The case with adjusted couplers, curve b.

The frequency band becomes much wider, while the system becomes less dispersive.

Figure 10 gives similar results for the detuned 204 cell structure. Figure 11 represents curves of the reflection coefficient $\mathcal{R}$ of this structure, with no adjusted couplers, for several different truncation numbers J^W. The curves tend to follow each other—the larger the truncation number, the smaller the differences. For $J^W > 30$, the difference in frequencies corresponding to the zeros of $\mathcal{R}$ is smaller then 1 MHz, corresponding to the relative accuracy of the frequency determination 10^{-4}. The full width of the resonance at the half maximum is ≈ 0.9 MHz. The resonances are spaced at approximately $\Delta f/N_c$, where Δf is the frequency width of the structure passband (in this case, an intermediate value between the widths of the passbands corresponding to the first and to the last cavities, see Fig. 2).

Figures 9 and 10 illustrate the action of couplers. Although the parameters of the couplers have been chosen at a particular frequency, they suppress the reflection of the EM wave in a rather broad band of frequencies.

6. ENERGY GAIN AND WAVE IMPEDANCE

In this Section we consider the acceleration of a test particle by a monochromatic travelling wave, with the frequency ω entering the structure from its left. In all the formulae, the terms arising due to the beam current must be omitted, i.e., N_B should be put to zero.

The propagation functions $x_n^N(z)$ and $\xi_n^N(z)$ define the longitudinal Fourier harmonic $E_z(r, z, k)$, with the wave number k (or the circular frequency $\omega \equiv kc$) at any point along the section [see Eqs. (2.1) and (2.4)]. After $x_n^N(z)$, $\xi_n^N(z)$ are

found, it is easy to calculate the total energy gain $\Delta\mathcal{E}(s)$ by a test particle with the initial position s:

$$\Delta\mathcal{E}(s) \;=\; \int_0^L dZ\; e\,E_z(0,Z,t)\Big|_{t\,=\,(Z-s)/c} \;. \tag{6.1}$$

The field $E_z(0,Z,t)$ can be found from its Fourier harmonics for all the frequencies Ω. For a monochromatic wave Eq. (4.5) the field in the mth cell is

$$\begin{aligned} E_z^m(0,Z,\Omega/c) \;&=\; 2\pi\;\exp\{i(\Omega/c)\,(s-Z^m)\}\;\sum\nolimits_{n=1}^{J^C}\;(\nu_n/d^m)^2 \\ &\times\;\Big[\;\widetilde{X}_n^m(z)\;\delta(\Omega-\omega)+\widetilde{X}_n^{m*}(z)\;\delta(\Omega+\omega)\;\Big]\;. \end{aligned} \tag{6.2}$$

Thus one finds

$$\Delta\mathcal{E}(s) \;=\; e\exp\{iks\}\;\sum\nolimits_{m=1}^{N_c}\;V^m(k)+\text{c.c.}\;, \tag{6.3}$$

where the voltage per cell is

$$V^m(k) \;=\; \sum\nolimits_{n=1}^{J^C}\;\exp\{-ikZ^m\}\;\int_0^{f^m} dz\;(\nu_n/d^m)^2\;\widetilde{X}_n^m(z)\;\exp\{-ikz\}\;. \tag{6.4}$$

In Eqs. (6.2) and (6.4), Z^m is the z-coordinate of the left end of the cavity or the iris of the mth cell, calculated from the beginning of the section. The radius d^m and the length f^m are understood to be those either of the mth cavity (b^m and g^m) or of the mth iris (a^m and l^m), respectively. Similarly, the propagation function $\widetilde{X}_n^m(z)$ is $x_n^m(z)$ in the mth cavity or $\xi_n^m(z)$ in the mth iris.

Due to the linearity of the Maxwell equations, the field everywhere in the section is proportional to the complex amplitude of the incident wave. We choose

to normalize the wave in the following way. In the straight beam pipe at the entrance to the section the incident wave has the form

$$E_z^1(r,z,\Omega/c) \;=\; \exp\{i(\Omega/c)s\}\;(\nu_1/b^1)^2\;J_0(\nu_1 r/b^1)\;[x_{\rm in}\;\delta(\Omega-\omega)+x_{\rm in}^*\;\delta(\Omega+\omega)]\;, \tag{6.5}$$

where

$$x_{\rm in} \;\equiv\; x_1^1(0) \;=\; \overrightarrow{C}_1^1+\overleftarrow{C}_1^1 \;=\; \overrightarrow{C}_1^1(1+\mathcal{R})\;. \tag{6.6}$$

The absolute value $|\overrightarrow{C}_1^1|$ is defined by the RF power of the incident monochromatic wave, see Eq. (4.6),

$$P(\omega) \;=\; \nu_1^2\;J_1^2(\nu_1)\;(\omega\lambda_1^1/2)\;|\,x_{\rm in}/(1+\mathcal{R})\,|^2\;. \tag{6.7}$$

The ratio $V^m/x_{\rm in}$ is independent of the amplitude of the incoming RF wave. Since the amplitude $x_{\rm in}$ is proportional to the square root of the incident power P, the energy gain is also proportional to $\sqrt{P}$.

The phase of $x_{\rm in}$ can be chosen with respect to s in such a way as to place a particle on the crest of the accelerating RF wave in the beginning of the section. This corresponds to maximum energy gain for each given frequency:

$$\Delta\mathcal{E}_{\rm max} \;=\; e\;|x_{\rm in}|\;\;|\,V(k)/x_{\rm in}\,|\;, \tag{6.8}$$

where the total accelerating voltage $V(k)$ for whole section is

$$V(k) \;\equiv\; \Delta\mathcal{E}_{\rm max}/e \;=\; \sum\nolimits_{m=1}^{N_c}\;V^m(k)\;. \tag{6.9}$$

It is useful to define the ratio:

$$Z_w(k) \;=\; (\Delta\mathcal{E}_{\rm max}/e)^2/\,P(\omega)\;, \tag{6.10}$$

which does not depend on the power of the incident wave. Substituting here $\Delta\mathcal{E}_{\max}$ from Eq. (6.9), one gets:

$$Z_w(k) \;=\; \{Z_0\,/\,[2\pi k\lambda_1\nu_1^2 J_1^2(\nu_1)]\}\;|1+\mathcal{R}|^2\;\left|\sum_{m=1}^{N_c}(V^m/x_{\rm in})\right|^2 . \qquad (6.11)$$

Here the free space impedance $Z_0 = 4\pi/c = 377\ \Omega$ is introduced. We call the quantity Z_w the wave impedance. It has the correct dimensions of Ω. For each given frequency, it is solely the characteristic of the structure. In terms of the wave impedance Z_w, the maximum energy gain by a test particle is

$$\Delta\mathcal{E}_{\max}\ (\mathrm{MeV}) \;=\; \sqrt{P\ (\mathrm{MW})\ Z_w\ (\mathrm{M}\Omega)}\ . \qquad (6.12)$$

Figure 11 represents the dependence of the wave impedance on the frequency of the incident wave for the 30-cell section, with and without couplers.

The action of couplers discussed in Section 5 are seen here once again. The maxima in the frequency dependence of the wave impedance for the unmatched section corresponds to the zeros of the reflection coefficient; cf., curve *a* on Fig. 9. In Fig. 12, the peaks in curve *a* (without the couplers) are narrower and higher than those in curve *b* for the section with the matched couplers . The unmatched section can give a higher acceleration rate at the frequency where the reflection coefficient is small. However, dispersive effects in this case are large, and transmission of a short RF pulse through such a section can be accompanied by big distortions. The adjustment of the couplers makes transmission of the EM wave effective in a rather broad band of frequencies of the order of 200 MHz, allowing a rise time of the RF pulse of the order of 5 nsec.

A similar situation can be seen in Fig. 13, which depicts the wave impedance for the unmatched (curve *a*) and the matched (curve *b*) 204-cell detuned structure.

Figures 14 and 15 represent the real and imaginary parts of the normalized energy gain $V^m/x_{\rm in}$ for the detuned structure for the mth cell versus number m. Three different frequencies of the incident wave were considered:

$f = 11.427$ MHz, below the pick of the wave impedance, which corresponds to the phase velocities below that of light $v_{\rm ph} < c$ for the equivalent infinitely periodic structures (curve a);

$f = 11.431$ MHz, $v_{\rm ph} \approx c$ (curve b); and

$f = 11.435$ MHz, $v_{\rm ph} > c$ (curve c).

For each frequency, the absolute value of the total accelerating voltage $|V|$, from Eq. (6.9), is given in the figure caption.

7. COUPLING IMPEDANCE, WAKE FUNCTION AND LOSS FACTOR

Now we turn to the problem of the excitation of the EM field in an aperiodic section by a particle beam current. In this case, the second term of each vector G_i^N, Eq. (A.46), should be omitted, $x_{\rm in} = 0$. The EM fields are defined by the first term in Eqs. (A.41) and (A.46) which is proportional to $\mathcal{F}(k)$. Since the Fourier harmonics of the beam current now contain a whole spectrum of frequencies, the solution for the EM field is the sum over all the relevant frequencies.

The total energy loss $\Delta\mathcal{E}$ experienced by a test particle moving on the trajectory $Z = ct + s$ due to the wakefield excited in the whole section by the beam is

$$\Delta\mathcal{E}(s) \;=\; \int_0^L dZ \int_{-\infty}^{\infty} [d\omega/2\pi]\; e\, E_z(0, Z, \omega)\; \exp\{-ik(Z-s)\}\;. \qquad (7.1)$$

Consider a train of n_b bunches, $l = 1, 2, \ldots, n_b$. Let $l = 1$ correspond to the bunch in the head of the train. It is convenient to write the factor $\mathcal{F}(k)$ in Eq. (2.14), explicitly omitting it from the definitions for G_i^N in Eq. (A.41) and (A.46).

The total energy loss of the test particle in the lth bunch of the train can be represented as the sum over individual cells

$$\Delta\mathcal{E}_l(s) \;=\; (2N_B e^2/\pi) \quad \sum\nolimits_{j\le l} \\ \times \Big[\int_{-\infty}^{\infty} dk \;\exp\{ik(s+s_l-s_j)\} \sum\nolimits_{m=1}^{N_c} \; V^m(k) + \text{c.c.} \Big] \,. \tag{7.2}$$

Here the dimensionless values $V^m(k)$, are defined by the same Eq. (6.4). But the propagation functions must certainly be calculated with the driving terms G_i^N arising from the beam current Eq. (2.2).

The wakefield is defined [19,20] by

$$w_l(s) \;=\; -\Delta\mathcal{E}(s) \;/\; (N_b\, e^2) \,. \tag{7.3}$$

For the lth bunch in a train, it can be represented as the convolution

$$w_l(s) \;=\; (2/Z_0) \int_{-\infty}^{\infty} dk \;\exp\{iks\} \; Z_c(k) \; \Phi_l(k) \tag{7.4}$$

of the longitudinal coupling impedance

$$Z_c(k) \;=\; -(Z_0/\pi) \sum\nolimits_{m=1}^{N_c} \; V^m(k) \tag{7.5}$$

and the form-factor

$$\Phi_l(k) \;=\; \sum\nolimits_{j\le l} \; a_{lj} \;\exp\{ik(s_l - s_j)\} \,, \tag{7.6}$$

where the coefficients $a_{l,j} = 1/2$ for $l = j$, and $a_{l,j} = 1$ otherwise.

The real and imaginary parts of the coupling impedance calculated for the 30-cell constant impedance section are depicted in Figs. 16 and 17, for the first and the second passbands, respectively. Similarly, the real and imaginary parts of the coupling impedance for the first passband of the 204-cell detuned section is drawn in Fig. 18.

The real part of the coupling impedance has a band structure with width Δf, corresponding to the filling time of a section $\Delta f \simeq 1/\tau_f$, where the filling time is defined by the group velocity v_g: $\tau_f \simeq L/v_g$. This can be expected for a traveling wave structure where $x_n(z)$ is, basically, a plane wave with the propagating constant $q = \psi/d$, ψ being the phase advance per cell and $d = L/N_c$ the period of the structure. The group velocity is then $v_g = d\omega/dq$. The real part of the impedance has the maximum at the frequency of the synchronous wave $q = k$ and the width $\Delta f = v_g \Delta q/2\pi$, where $\Delta q \simeq 2\pi/L$. The total energy loss is proportional to $\int Z(k)dk$, and changes little with small variations of the cell dimensions. Therefore, the maximum value of the impedance is inversely proportional to Δf, and increases with decreasing v_g.

The developed formalism gives the energy loss for any particle distribution inside the bunch and for any bunch distribution in the train. For the equidistant train in which bunches are equally spaced at distance s_b, the form factor Eq. (7.6) can be found explicitly:

$$\Phi_l(k) \;=\; (1/2) + \exp\{iq_b l\}\;[\sin q_b(l-1)/\sin q_b]\;, \tag{7.7}$$

where $q_b \equiv ks_b/2$. If $l \gg 1$, the form factor is close to δ function

$$\Phi_l(k) \;=\; (\pi/s_b)\;\delta\,[k - (2\pi l\,/\,s_b)] \tag{7.8}$$

For a short bunch with *rms* length $\sigma_b \ll s_b$, the maximum energy loss due to the interaction with the wakefield is

$$\Delta\mathcal{E}_{\rm loss} \;=\; (4N_B e^2/s_b)\;\sum\nolimits_{m=1}^{N_c}\;{\rm Re}\,V^m\;(2\pi l/s_b)\;. \tag{7.9}$$

All the integers l such that the corresponding wave number $k = 2\pi l/s_b$ happens to be inside the passband give additive contribution to $\Delta\mathcal{E}_{\rm max}$. If s_b is not

too large, only one value of the integer l contributes to $\Delta\mathcal{E}_{\max}$. It is convenient to express the maximum energy loss in the section in terms of the beam loading parameter

$$B_L(\mathrm{MeV}) \;=\; 5.6\times 10^{-3}\;\sum_{m=1}^{N_c}\;\mathrm{Re}\,V^m\;. \tag{7.10}$$

In terms of this parameter, the maximum energy loss experienced by a particle on a plateau of the beam loading curve in a long train of bunches, with bunch spacing s_b, is

$$\Delta\mathcal{E}_{\mathrm{loss}}\;(\mathrm{MeV}) \;=\; (N_B/10^{10})\;[B_L\;(\mathrm{MeV})\;/\;s_b(cm)]\;. \tag{7.11}$$

In Fig. 19 the beam loading parameter B_L is plotted as a function of frequency for the 204-cell section with adjusted couplers. Curve a is calculated for the detuned section, and curve b for a constant impedance section with the dimensions of the first cell of the detuned section. The maximum value of B_L is proportional to the maximum value of the coupling impedance. It is smaller for the first cell (for which v_g is large) then for an average cell; see Fig. 2.

Figure 20 represents the beam loading parameter B_L in function of frequency for the 30-cell constant impedance section with adjusted couplers. In Fig. 20(a) B_L is plotted for the first, in Fig. 20(b) for the second passband, respectively.

Another characteristic of a structure, namely the loss factor κ, is also easy to calculate using Eq. (7.4)

$$\kappa \;=\; \int_{-\infty}^{\infty}\;(d\omega/2\pi)\;Z_c(\omega)\;. \tag{7.12}$$

Integrating the curves in Figs. 16(a) and 19(a) over the frequency we obtained $\kappa = 60.773$ V/pC for the 30-cell periodic section (or ≈ 2.03 V/pC per cell) and $\kappa = 389.59$ V/pC for the 204-cell detuned section (or ≈ 1.91 V/pC per cell).

8. CONCLUSION

The developed method and the numerical code *PROGON* based on it are demonstrated to give answers to a wide range of problems pertaining to the propagation and excitation of the EM fields in the disc-loaded aperiodic structures. For the time being, they are limited to longitudinal axially-symmetric problems. However, the extension of the formalism onto transverse fields is straightforward and can be used to find the transverse wakefields in detuned structures.

ACKNOWLEDGEMENTS

Discussions with several people greatly contributed to this work. We are grateful to all of them, and especially to K. Bane, K. Ko, R. Miller, B. Littman, E. Nelson, R. Ruth, J. Wang and M. Zolotarev. Our special gratitude goes to A. Kheifets from Kharkov, Ukraine.

APPENDIX: BASIC EQUATIONS

Here we derive the basic system of algebraic equations for the field amplitides. The kth Fourier harmonics of the EM field in the region inside of the Nth cavity with constant radius b^N can be expanded in the spatial modes

$$E_z^N(r,z,k) = \sum_{n=1}^{\infty} (\nu_n/b^N)^2 \, J_0(\nu_n r/b^N) \, x_n^N(z) \,, \qquad (A.1)$$

$$E_r^N(r,z) = (2eN_B/cr) \sum_j \exp\{ik(Z-s_j)\} - \sum_{n=1}^{\infty} (\nu_n/b^N) \, J_1(\nu_n r/b^N) \, y_n^N(z) \,, \qquad (A.2)$$

$$H_\phi^N(r,z) = (2eN_B/cr) \sum_j \exp\{ik(Z-s_j)\} - ik \sum_{n=1}^{\infty} (\nu_n/b^N) \, J_1(\nu_n r/b^N) \, x_n^N(z) \,, \qquad (A.3)$$

where the propagation functions $x_n^N(z)$, $0 < z < g^N$ and

$$y_n^N(z) = dx_n^N(z)/dz \,, \qquad 0 < z < g^N \qquad (A.4)$$

describe the z dependence of the nth spatial mode in the Nth cavity.

Similarly, for the Nth iris with the radius a^N

$$E_z^N(r,z) = \sum_{n=1}^{\infty} (\nu_n/a^N)^2 \, J_0(\nu_n r/b^N) \, \xi_n^N(z) \,, \qquad (A.5)$$

$$E_r^N(r,z) = (2eN_B/cr) \sum_j \exp\{ik(Z-s_j)\} - \sum_{n=1}^{\infty} (\nu_n/a^N) \, J_1(\nu_n r/a^N) \, \mu_n^N \eta_n^N(z) \,, \qquad (A.6)$$

with the propagation functions $\xi_n^N(z)$, $0 < z < l^N$, and

$$\eta_n^N(z) = (1/\mu_n^N) \left[d\xi_n^N(z) \Big/ dz \right] \,, \qquad 0 < z < l^N \,. \qquad (A.7)$$

In the above expressions, we distinguish between the longitudinal coordinate of the bunch Z calculated from an arbitrary point (for example, from the beginning

of the structure) and the local longitudinal coordinate z in the cavity or the iris calculated from the left side of each region.

Each of the propagation functions is a superposition of two waves travelling in $+z$ (forward wave) or in $-z$ (backward wave) directions:

$$x_n^N(z) \;=\; \overrightarrow{C}_n^N \;\exp\left\{i\lambda_n^N z\right\} \;+\; \overleftarrow{C}_n^N \;\exp\left\{-i\lambda_n^N z\right\}\;, \tag{A.8}$$

$$\xi_n^N(z) \;=\; \overrightarrow{D}_n^N \;\exp\left\{i\mu_n^N z\right\} \;+\; \overleftarrow{D}_n^N \;\exp\left\{-i\mu_n^N z\right\}\;, \tag{A.9}$$

The phases of the complex amplitudes $\overrightarrow{C}_n^N$, $\overleftarrow{C}_n^N$, $\overrightarrow{D}_n^N$ and $\overleftarrow{D}_n^N$ are defined by choosing $z = 0$ at the left side of each cavity or iris. $\nu_n, n = 1, 2, \ldots$ are the roots of the first order Bessel function $J_0(\nu_n) = 0$ arranged in ascending order $\nu_1 < \nu_2 < \ldots$. Further, the propagation constants

$$\mu_n^N \;=\; \sqrt{k^2 - (\nu_n/a^N)^2}\;, \tag{A.10}$$

$$\lambda_n^N \;=\; \sqrt{k^2 - (\nu_n/b^N)^2}\;, \tag{A.11}$$

are defined with a cut in the complex plane k in such a way as to ensure the radiation condition at $\pm\infty$. For example,

$$\mu_n^N(-k^*) \;=\; -\mu_n^{N*}(k)\;. \tag{A.12}$$

The continuity Eqs. (2.10-11) give the following relations between the propagation functions:

$$\begin{aligned} y_m^{N-1}(g^{N-1}) \;=\; (4eN_B/c) \;\; & \left[J_0(\nu_n p^{N-1}) \,\Big/\, \nu_n^2 J_1^2(\nu_n)\right] \\ & \times \sum\nolimits_j \exp\left\{ik(Z^N - s_j)\right\} - \sum\nolimits_n T_{mn}(p^{N-1})\;\eta_n^N(0)\;, \end{aligned} \tag{A.13}$$

$$\xi_n^N(0) \;=\; -\sum\nolimits_m S_{nm}(p^{N-1})\;x_n^{N-1}(g^{N-1})\;, \tag{A.14}$$

$$\xi_n^N(l^N) \;=\; \sum\nolimits_m S_{nm}(p^N)\;x_n^N(0)\;, \tag{A.15}$$

$$y_m^N(0) \;=\; (4eN_B/c)\;\Big[J_0(\nu_n p^N)\Big/\,\nu_n^2 J_1^2(\nu_n)\Big] \times \sum\nolimits_j \exp\Big\{ik(Z^N - s_j)\Big\} \;-\sum\nolimits_n T_{mn}(p^N)\;\eta_n^N(l^N)\;, \tag{A.16}$$

where $p^N \equiv a^N/b^N$ and $p^{N-1} \equiv a^N/b^{N-1}$, respectively.

The elements of the matrices S and T are defined as follows:

$$S_{nm}(p) \;=\; \big[2p^2\nu_m^2\;J_0(p\nu_m)\big]\big/\,\big[\,\nu_n\;J_1(\nu_n)\;(\nu_n^2 - p^2\nu_m^2)\big]\;, \tag{A.17}$$

$$T_{mn}(p) \;=\; \big[2p^2\nu_n\mu_n\;iJ_1(\nu_n)\;J_0(p\nu_m)\big]\big/\,\big[\,J_1^2(\nu_m)\;(\nu_n^2 - p^2\nu_m^2)\big]\;. \tag{A.18}$$

Note that all the matrices S and T are real.

The iris variables can be excluded altogether. Indeed, from Eqs. (A.7-9) it follows that

$$\eta_n^N(0) \;=\; -\;i\xi_n^N(0)\Big/\,\tan\alpha_n^N \;+\; i\xi_n^N(l^N)\Big/\,\sin\alpha_n^N\;, \tag{A.19}$$

$$\eta_n^N(l^N) \;=\; -\;i\xi_n^N(0)\Big/\,\sin\alpha_n^N \;+\; i\xi_n^N(l^N)\Big/\,\tan\alpha_n^N\;, \tag{A.20}$$

where $\alpha_n^N = l^N\mu_n^N$. The quantities $\xi_n^N(0)$ and $\xi_n^N(l^N)$ are given by Eqs. (A.14) and (A.15). Substitution of Eqs. (A.19) and (A.20) into Eqs. (A.13) and (A.16) gives

$$\begin{aligned} y_n^{N-1}(g^{N-1}) \;&=\; (4eN_B/c)\;\Big\{J_0(\nu_n p^{N-1})\Big/\,\big[\nu_n^2\;J_1^2(\nu_n)\big]\Big\} \\ &\quad\times \sum\nolimits_j \exp\Big\{ik\Big[Z^{N-1}(g^{N-1}) - s_j\Big]\Big\} \\ &\quad-\sum\nolimits_k Q_{nk}^{N-1,N-1}\;x_k^{N-1}(g^{N-1}) \\ &\quad+\sum\nolimits_k R_{nk}^{N-1,N}\;x_n^N(0)\;, \end{aligned} \tag{A.21}$$

$$\begin{aligned} y_n^N(0) \;&=\; (4eN_B/c)\;\Big\{J_0(\nu_n p^N)\Big/\,\big[\nu_n^2\;J_1^2(\nu_n)\big]\Big\} \\ &\quad\times \sum\nolimits_j \exp\Big\{ik\Big[Z^N(0) - s_j\Big]\Big\} \\ &\quad+\sum\nolimits_k Q_{nk}^{N,N}\;x_k^N(0) \;-\sum\nolimits_k R_{nk}^{N,N-1}\;x_n^{N-1}(g^{N-1})\;, \end{aligned} \tag{A.22}$$

where

$$Q_{nk}^{N,M} \;=\; -i\sum\nolimits_m \left(T_{nm}^N \; S_{mk}^M / \tan\alpha_m^N\right) , \qquad (A.23)$$

$$R_{nk}^{N,M} \;=\; -i\sum\nolimits_m \left(T_{nm}^N S_{mk}^M / \sin\alpha_m^N\right) . \qquad (A.24)$$

For most of the terms in the sums in Eqs. (A.23-24) with large indices m, α_m^N are purely imaginary. The contribution of such terms decreases rather rapidly.

The system Eqs. (A.21-22) can be written in the matrix form for the vector $y^N(0) \equiv \{y_1^N, y_2^N, \ldots\}$, and similarly defined vectors $y^{N-1}(g^{N-1})$, $x^N(0)$ and $x^{N-1}(g^{N-1})$,

$$y^{N-1}(g^{N-1}) \;=\; P^{N-1}(p^{N-1}) + R^{N-1,N}\; x^N(0) - \; Q^{N-1,N-1}\; x^{N-1}(g^{N-1}) , \qquad (A.25)$$

$$y^N(0) \;=\; P^N(p^N) + Q^{N,N}\; x^N(0) - R^{N,N-1}\; x^{N-1}(g^{N-1}) , \qquad (A.26)$$

where

$$P_n^{N-1}(p^{N-1}) \;=\; \mathcal{F}(k)\; \left\{ J_0(\nu_n p^N) \Big/ \left[\nu_n^2\, J_1^2(\nu_n)\right]\right\} \times\; \exp\left\{ ik \sum\nolimits_{m=1}^{N-1} (g^m + l^m) - ikl^{N-1}\right\} , \qquad (A.27)$$

$$P_n^N(p^N) \;=\; \mathcal{F}(k)\; \left\{ J_0(\nu_n p^N) \Big/ \left[\nu_n^2\, J_1^2(\nu_n)\right]\right\} \times\; \exp\left\{ ik \sum\nolimits_{m=1}^{N-1} (g^m + l^m)\right\} . \qquad (A.28)$$

In the last two equations the following function has been introduced

$$\mathcal{F}(k) \;\equiv\; (4eN_B/c) \sum\nolimits_j \exp\{-iks_j\} , \qquad (A.29)$$

which describes the excitation of the system by a train of bunches.

The vectors $x^N(g^N)$, $y^N(g^N)$ can be expressed in terms of vectors $x^N(0)$, $y^N(0)$. Then Eqs. (A.25-26) give a set of linear algebraic equations for $x^N(0)$, $y^N(0)$

which in turn give the vectors $x^N(0)$, $y^N(0)$ for $N = 2, 3, \ldots N_c$ in terms of the vectors $x^1(0)$, $y^1(0)$ at the first iris. However, such a direct approach is numerically unstable, and does not provide the solution for any structure consisting of more then a few cells. The reason for this is that the relation of the quantities $x^N(0), y^N(0)$ at the beginning of the Nth cell, and $x^{N+1}(0), y^{N+1}(0)$ at the beginning of the next cell, contain evanescent modes. Some of them might be exponentially large or small. As a result, numerical errors in such an approach grow exponentially along the structure.

To find a numerically stable solution of the problem for an aperiodic structure we exclude the vectors $y^N(g^N)$ and $y^N(0)$:

$$y^N(0) \;=\; -\,\lambda^N\, x^N(0)\Big/\tan\beta^N \;+\; \lambda^N\, x^N(g^N)\Big/\sin\beta^N\;, \quad (A.30)$$

$$y^{N-1}(g^{N-1}) \;=\; \lambda^{N-1}\, x^{N-1}(g^{N-1})\Big/\tan\beta^{N-1} - \;\lambda^{N-1}\, x^{N-1}(0)\Big/\sin\beta^{N-1}\;, \quad (A.31)$$

where $\beta^N = g^N\lambda^N$. These expressions are valid for all irises, with the exception of the first and last ones. The conditions on the end irises are different, and are given by Eqs. (4.3-4) in Section 4.

Note that Eqs. (A.30-31) do not contain large exponents. This situation is similar to that in the standard S-matrix formalism. For the evanescent modes, the last terms are exponentially small and the first terms relate the value of the propagation function y of the radial component E_r of the field to the value of the propagation function x of the longitudinal component E_z on the same iris. This seems to be reasonable from the physics of the problem—elimination of the large exponents is crucial for the stability of the numerical calculations.

From Eqs. (A.25-26) then follows the system of linear algebraic equations for the values of the propagation functions $x_n^N(0)$ and $x_n^{N-1}(g^{N-1})$:

$$P_n^{N-1}\,(p^{N-1}) \;=\; -\sum\nolimits_{k=1} R_{nk}^{N-1,N}\; x_k^N(0) - \left[\lambda_n^{N-1} \Big/ \sin\beta_n^{N-1}\right]\; x_n^{N-1}(0)$$

$$+\; \sum\nolimits_{k=1} \left\{ Q_{nk}^{N-1,N-1} + \delta_{nk}\; \left[\lambda_n^{N-1} \Big/ \tan\beta_n^{N-1}\right]\right\}\; x_k^{N-1}\,(g^{N-1})\,, \quad (A.32)$$

$$P_n^N(p^N) \;=\; -\sum\nolimits_{k=1} \left[Q_{nk}^{N,N} + \left(\lambda_n^N \Big/ \tan\beta_n^N\right)\; \delta_{nk}\right]\; x_k^N(0)$$

$$+\; \sum\nolimits_{k=1} R_{nk}^{N,N-1}\; x_k^{N-1}(g^{N-1}) + \left(\lambda_n^N \Big/ \sin\beta_n^N\right)\; x_n^N(g^N)\,. \quad (A.33)$$

The system of Eqs. (A.32-33) will be solved by truncation, keeping only the first J^C spatial modes in the cavities.

We introduce the set of $N_c - 1$ vectors f_i^N, $\quad i = 1, 2, \ldots, 2J^C$, of the rank $2J^C$ which describe the field on both sides of the Nth iris:

$$f_i^N \;\equiv\; x_i^N(0)\,, \qquad i = 1, \ldots, J^C\,, \quad (A.34)$$

$$f_{i+J}^N \;\equiv\; x_i^{N-1}(g^{N-1})\,, \qquad i = 1, \ldots, J^C\,. \quad (A.35)$$

Equations (A.32-33) can now be written in the form of recurrent equations:

$$A^N\, f^N \;=\; B^N\, f^{N-1} + F^N\, f^{N+1} + G^N\,, \qquad N = 2, 3, \ldots, N_c\,, \quad (A.36)$$

where all the elements of the matrices A^N, B^N, F^N of the rank $2J^C \times 2J^C$ and G^N of the rank $2J^C$ are:

For the elements with indices $i = 1, \ldots, J^C, (n \equiv i)$**:**

$$A_{ij}^N \;=\; -\,Q_{nk}^{N,N} - \left[\lambda_n^N \Big/ \tan\beta_n^N\right]\; \delta_{nk} + \left[\lambda_n^{N_c} \Big/ \sin\beta_n^{N_c}\right]$$

$$\times\; \delta_{NN_c}\, \delta_{ij}\, \exp\left\{i\beta_n^{N_c}\right\}\;;\quad j = 1, 2, \ldots, J^C;\quad k = j\;; \quad (A.37)$$

$$A_{ij}^N \;= R_{nk}^{N,N-1}\;;\quad j = J^C + 1, \ldots, 2J^C\;;\quad k = j - J^C\;; \quad (A.38)$$

$$B_{ij}^N = 0\,; \quad j = 1, 2, \ldots, 2J^C\,; \tag{A.39}$$

$$F_{ij}^N = -\left(\lambda_n^N \Big/ \sin\beta_n^N\right)\, \delta_{j,n+J^C}(1-\delta_{NN_c})\,; \quad j = 1, 2, \ldots, 2J^C\,; \tag{A.40}$$

$$G_i^N = \mathcal{F}(k)\, \left\{ J_0(\nu_n p^N) \Big/ \left[\nu_n^2 J_1^2(\nu_n)\right]\right\} \exp\left\{ik(N-1)(g^N + l^N)\right\} \tag{A.41}$$

For the elements with indices $i = J^C + 1, \ldots, 2J^C$, $(n \equiv i - J^C)$**:**

$$A_{ij}^N = -R_{nk}^{N-1,N}\,; \quad j = 1, \ldots, J^C\,; \quad k = j\,; \tag{A.42}$$

$$\begin{aligned} A_{ij}^N &= Q_{nk}^{N-1,N-1} + \left(\lambda_n^{N-1} \Big/ \tan\beta_n^{N-1}\right)\, \delta_{ij} \\ &\quad - \delta_{ij}\, \delta_{N2}\, \left(\lambda_n^1 / \sin\beta_n^1\right)\, (1 - \delta_{n1} + \delta_{n1}\delta_{N_B})\, \exp\left\{i\beta_n^1\right\}\,, \\ &\qquad j = J^C + 1, \ldots, 2J^C\,; \quad k = j - J^C\,; \end{aligned} \tag{A.43}$$

$$B_{ij}^N = \left(\lambda_n^{N-1} \Big/ \sin\beta_n^{N-1}\right)(1-\delta_{N2})\, \delta_{nj}\,, \quad j = 1, \ldots, J^C\,; \tag{A.44}$$

$$F_{ij}^N = 0 \tag{A.45}$$

$$\begin{aligned} G_i^N &= \mathcal{F}(k)\left\{ J_0(\nu_n\, p^{N-1}) \Big/ \left[\nu_n^2\, J_1^2(\nu_n)\right]\right\} \\ &\quad \times \exp\left\{ik(N-1)(g^{N-1} + l^{N-1}) - ikl^{N-1}\right\} \\ &\quad + \left(\lambda_n^1 / \sin\beta_n^1\right)\, \delta_{N2}\, \delta_{n1}\, x_{\text{in}}(1-\delta_{N_B})\,. \end{aligned} \tag{A.46}$$

The Kronecker symbols with double indices have their usual meaning. The delta symbol with one index is defined as $\delta_{N_B} = 0$ when $N_B = 0$; $\delta_{N_B} = 1$ otherwise. The value x_{in} in Eq. (A.46) is defined by the power of the incoming RF wave.

Equations (A.36) for vectors f^N define the field in the structure. Apart from truncation to a finite J^C, they are exact. Note that the number of modes J^W

taken into account in the iris regions define only the accuracy of calculation of the sums (A.23-24). The choice of J^W depends only on the rate of convergence of the sums, and in no way is it related to the choice of the maximum number of modes in the cavities J^C.

Let us look at the system (A.36) more closely. If one neglects exponentially small terms F^N, the system Eq. (A.36) simplifies

$$A^N f^N = B^N f^{N-1} + G^N . \qquad (A.47)$$

Note that in this approximation the field on the Nth iris f_i^N, $i = 1, 2, \ldots, 2J^C$ is defined solely by its value on the preceding iris f_i^{N-1}. In this approximation, the evanescent modes are induced locally at each iris to compensate for the radial component of the propagating mode on the conductive surface of the iris.

The problem Eq. (A.47), as well as the starting problem, Eqs. (A.25-26), together constitute the Cauchi problem: the field in all of the system is defined by the field f_i^1 at the entrance. The exact Eqs. (A.36) include exponentially small corrections to the field on each iris arising from the evanescent fields of the neighboring irises. Using Eqs. (A.30-31), all the large exponents are eliminated from Eq. (A.36). The price for this is the transition from the Cauchi problem to a boundary-value problem for which the field is defined by the conditions on both the entrance and the exit of the system. This is the reason for the choice of the vectors f^N.

Given the conditions at the ends of the section, the system Eqs. (A.36) can be solved by the method of Gaussian elimination and back substitution [21,22]. In the Soviet mathematical literature this method has the name *progonka*.

Suppose that the solution for the vector f^N has the form

$$f^{N+1} = \mathcal{A}^N f^N + \mathcal{B}^N , \qquad (A.48)$$

with as yet unknown matrices $\mathcal{A}^N$ and $\mathcal{B}^N$. Substituting this relation into Eq. (A.36), solving it with respect to f^N, and comparing the coefficients yields the following recurrence equations for the matrices $\mathcal{A}^N$ and $\mathcal{B}^N$:

$$\mathcal{A}^{N-1} = (A^N - F^N \mathcal{A}^N)^{-1} B^N \,, \tag{A.49}$$

$$\mathcal{B}^{N-1} = (A^N - F^N \mathcal{A}^N)^{-1} (F^N \mathcal{B}^N + G^N) \,. \tag{A.50}$$

The last two relations allow determination of all $\mathcal{A}^N$ and $\mathcal{B}^N$ sequentially, provided the matrices $\mathcal{A}^{N_c}$ and $\mathcal{B}^{N_c}$ are known from the conditions on the right hand side of the system. After that, Eq. (A.48) gives the solution f^N, sequentially, provided again that f^1 is known from the conditions on the left-hand side of the system; see the discussion in Sec. 4.

REFERENCES

1. H. Deruyter et al., "Damped and Detuned Accelerator Structures," Proc 1990 Linear Accel. Conf., Albuquerque, NM, p. 132, 1990.
2. J. W. Wang, "Wakefield Measurements and Accelerator Structure Studies," SLAC/AAS Note 61, April 1991.
3. K. A. Thompson, J. W. Wang, "Simulation of Accelerating Structures with Large Staggered Tuning," IEEE Particle Accel Conf., San Francisco, May 6–9, 1991.
4. J. W. Wang and B. W. Littman, "Design Study on Quasi-Constant Gradient Accelerator Structure ," SLAC/AP–92 (1991).
5. E. Keil, "Diffraction Radiation of Charged Rings Moving in a Corrugated Cylindrical Pipe," Nucl. Instrum. Methods **100**, 419 (1972);
   E. Keil and B. Zotter, "The Coupling Impedance of Corrugated Vacuum Chambers: Several Cavities in a Period," CERN/ISR/TH–71–15 (1971).
6. T. Weiland, "On the Computation of Resonant Modes in Clylindrically Symmetric Cavities," Nucl. Instrum. Methods **216**, 329–348 (1983).
7. K. Halbach and R. F. Holsinger, "SUPERFISH—A Computer Programm for Evaluation of RF Cavities with Clyndrical Symmetry," Part. Accel. **7**, 213–222 (1976).
8. M. Drevlak, "Damfung von Transversalen Moden durch Variable Cellgeometrieen in Wanderwellenröhren," Thesis, Technische Hochschule Darmstadt, Darmstadt, Germany, 1991.
9. K. Bane and N. Holtkamp, "A Circuit Model for Obtaining the Coupled Dipole Modes of the NLC Accelerator Structure," SLAC/AAS Note 63 (1991).
10. K. Bane and R. Gluckstern, "The Transverse Wakefield of a Detuned X-Band Accelerator Structure," SLAC–PUB–5783 (1992).

11. S. A. Kheifets, "Longitudinal Impedance of Simple Cylindrically Symmetric Structures," IEEE Trans. Microwave Theory and Tech., **MTT–35**, No. 8, 753–760 (1987).
12. S. A. Kheifets, K. L. F. Bane and H. Bizek, "Transverse Impedances of Cavities and Collimators," Proc. 1987 Part. Accel. Conf., Washington D.C., March 16-19, 1987.
13. Tatsuo Itoh, "Numerical Techniques for Microwave and Millimeter-Wave Passive Structures," John Wiley and Sons, 1989.
14. R. Mitra, "Relative Convergence of the Solution of a Doubly Infinite Set of Equations," Jour. Research Nat. Bureau of Stand. D, Radio Propagation **67D**, No. 2, 1963, pp. 245–254.
15. S. A. Heifets and S. A. Kheifets, "Coupling Impedance in Modern Accelerators," Rev. Mod. Phys., **63**, No. 3, 631–673, 1991.
16. R. Miller, private communication.
17. J. Wang and B. W. Littman provided the results of their calculation.
18. S. A. Heifets and S. A. Keifets, in preparation.
19. K.F.L. Bane and P. B. Wilson, "Longitudinal and Transverse Wake Potentials in SLAC," Proc. 11th Int. Conf. on High-Energy Accel., Geneva, Switzerland, 1980, ed., W. S. Newman (Birkhauser Verlag, Basel), pp. 592-596.
20. K.F.L. Bane, "Wakefield Effects in Linear Colliders," SLAC–PUB–4169 (1986).
21. A. A. Samarskii and E. S. Nikolaev, "Numerical Methods of Grid Equations," **1** (Birkhauser Verlag, Basel–Boston–Berlin, 1989), p. 65.
22. A. A. Samarskii, "The Theory of Difference Schemes," (Nauka, Moscow, 1983) p. 35 (in Russian).

Table 1. Cell geometry.
All dimensions are in cm;
iris thickness $l = 0.146$ cm.

Cell Number	a	b	g
30-cell constant-impedance section			
1–30 (any cell)	0.375	1.059	0.729
2 (left coupler)	0.518	1.088	0.606
29 (right coupler)	0.528	1.088	0.606
204-cell detuned section			
1 (first)	0.543	1.121	0.729
102 (middle)	0.458	1.081	0.729
204 (last)	0.385	1.053	0.729
2 (left coupler)	0.691	1.115	0.902
203 (right coupler)	0.534	1.061	0.900

FIGURE CAPTIONS

1. Geometry and the coordinate system. The 30-cell constant inpedance section with couplers is taken as an illustration.
2. Dispersion curves for an infinite array of cells built of the first, the middle and the last cells of the 204-cell detuned accelerating section, see Table 1 for the cell geometry. The results of the calculations using the program *PROGON* are shown by symbols for the first (•), for the middle (○), and for the last (◇) cell.
3. Behavior of the dispersion curve with respect to the cavity truncation number J^C. The calculations for the first cell (see Table 1) of the detuned section has been done with $J^C = 4$ (□), 8 (■), 12 (○), 16 (•), 20 (◇), and 24 (◆). The dispersion curves tend to converge to the same curve with increasing J^C. The corresponding iris truncation number $J^W = 50$.
4. Behavior of the same curve as in Fig. 3, but for different iris trunction numbers $J^W = 16$, 24, 32, and 50. The cavity truncation number $J^C = 16$. All the results fit onto the same curve.
5. The blowup of the part of Fig. 3 from which the resonance frequency corresponding to the wave phase velocity equal to that of light was measured: $f = 11.421$ GHz for $J^C = 24$. Symbol notations given in the caption for Fig. 3.
6. Dispersion curves in the first (curve b) and the second (curve a) passbands of the 30-cell constant inpedance section. $J^C = 20$; $J^W = 30$.
7. An illustration of the continuity of the calculated radial electric field for the 30-cell constant impedance section (see Table 1). The real and imaginary parts of $E_r(r)$ are plotted as functions of the ratio r/b at the surface $z = l$ of one of the irises. The dashed line indicates the relative radius of the iris

aperture, a/b. Two curves in the region $r < a$ in each picture represent $E_r(r)$ at $z = l \pm 0$; $J^C = 24$; $J^W = 30$.

8. An illustration of the continuity of the calculated longitudinal electric field $E_z(z)$ on the axis of the same section as in Fig. 7. The absolute value (curve a) and the phase (curve b) of $E_z(z)$ on the section axis are plotted.
9. The absolute values of the reflection $|\mathcal{R}|$ and transmission $|\mathcal{T}|$ coefficients for the same section as in Fig. 7. Curves a represent the results of calculations for the section without and curves b with couplers. The geometry of couplers is given in Table 1.
10. The same as in Fig. 9, but for the 204-cell detuned accelerating section.
11. Behavior of the reflection $|\mathcal{R}|$ and transmission $|\mathcal{T}|$ coefficients with respect to the iris truncation number J^W plotted with the blowup of one of the peaks from Fig. 10. The curves are calculated with $J^C = 24$; $J^W = 30$ (•), 40 (◇), 50 (□), and 75 (○). The position of the minimum of $|\mathcal{R}|$ tends to converge to $f = 11.421$ GHz (cf., Fig. 5).
12. The wave impedance $Z_w(f)$ for the same section as in Fig. 7. Curve a represents the result of calculations for the section without and curve b with couplers (see Table 1).
13. The same as in Fig. 12, but for the 204-cell detuned accelerating section.
14. The real part of the voltage V^m in each cell of the 204-cell detuned section with couplers calculated for three typical frequencies (see text). The absolute values of the total voltage in arbitrary units are 1331.44 (curve a), 1818.21 (curve b), and 1265.16 (curve c).
15. The same as in Fig. 14, but for the imaginary part.
16. The real (a) and imaginary (b) parts of the coupling impedance $Z_c(f)$ in the first passband of the 30-cell constant impedance section with couplers.
17. The same as in Fig. 16, but in the second passband.

18. The same as in Fig. 16, but for the 204-cell detuned accelerating section.

19. The beam loading parameter $B_L(f)$ for the 204-cell section in two cases: (1) detuned (curve a) and (2) constant impedance built of repeated first cell (curve b). In the second case, v_g is larger, and the corresponding peak in $B_L(f)$ is lower and wider.

20. The beam loading parameter $B_L(f)$ for the 30-cell constant impedance section. Curve a is calculated for the first and curve b for the second passbands.

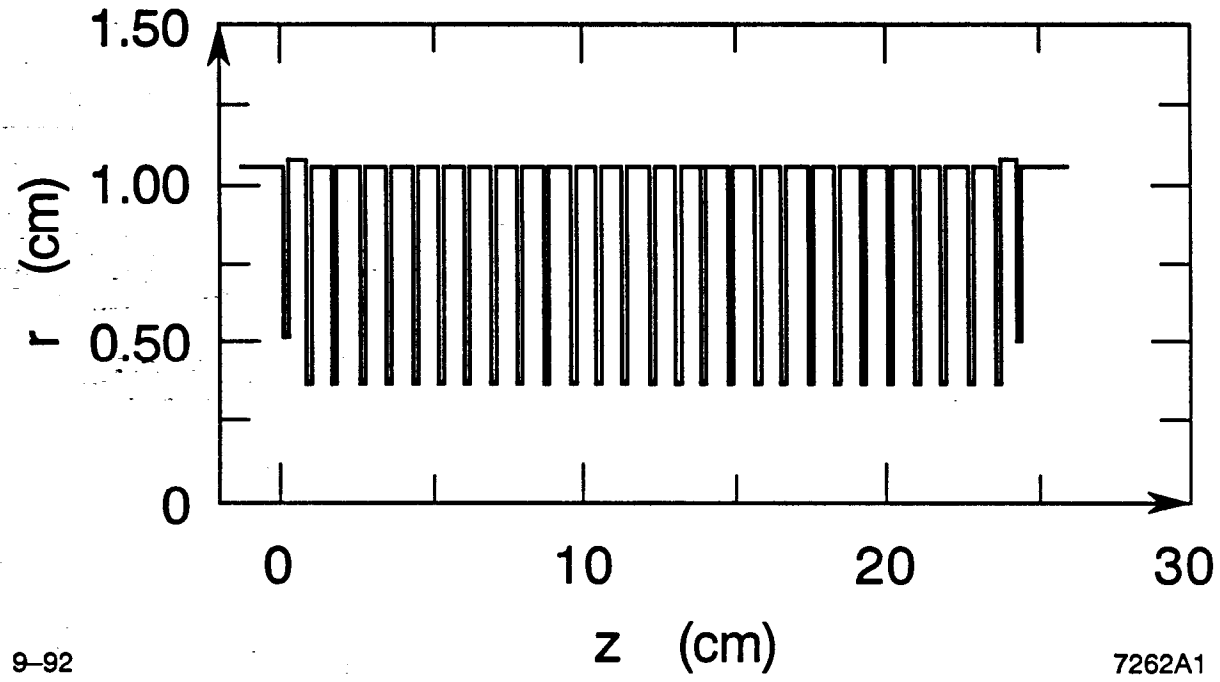

Fig. 1

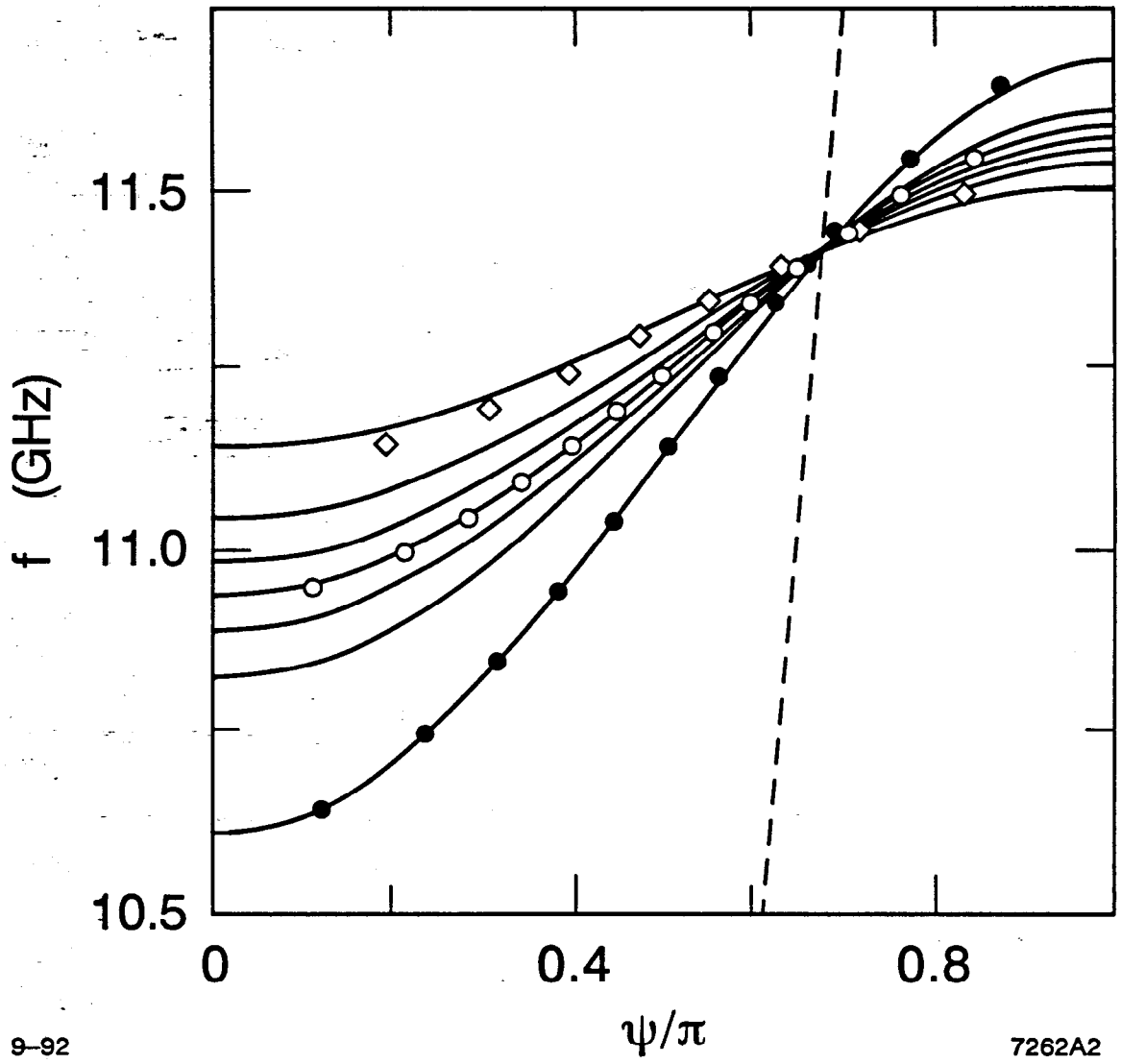

Fig. 2

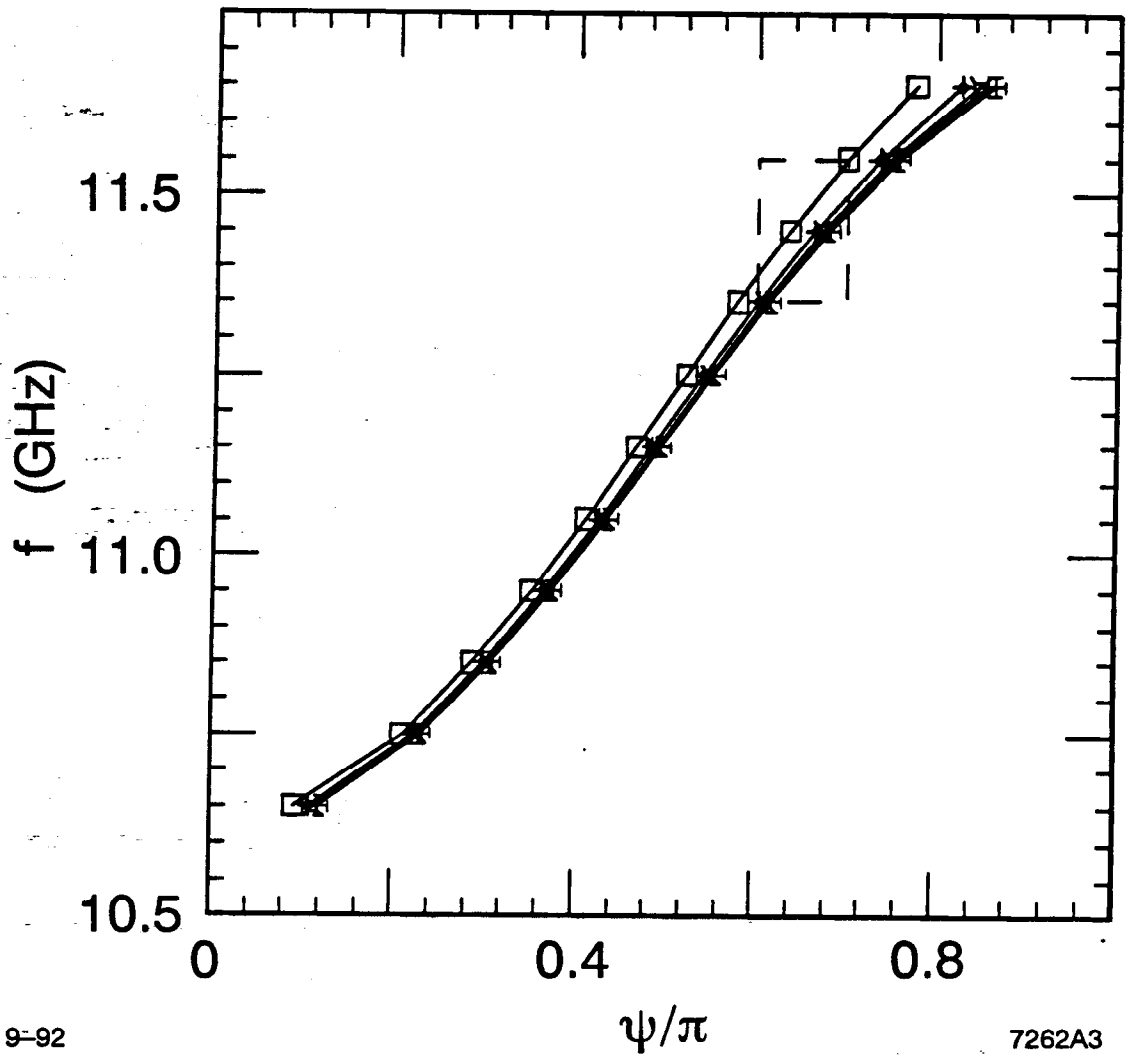

Fig. 3

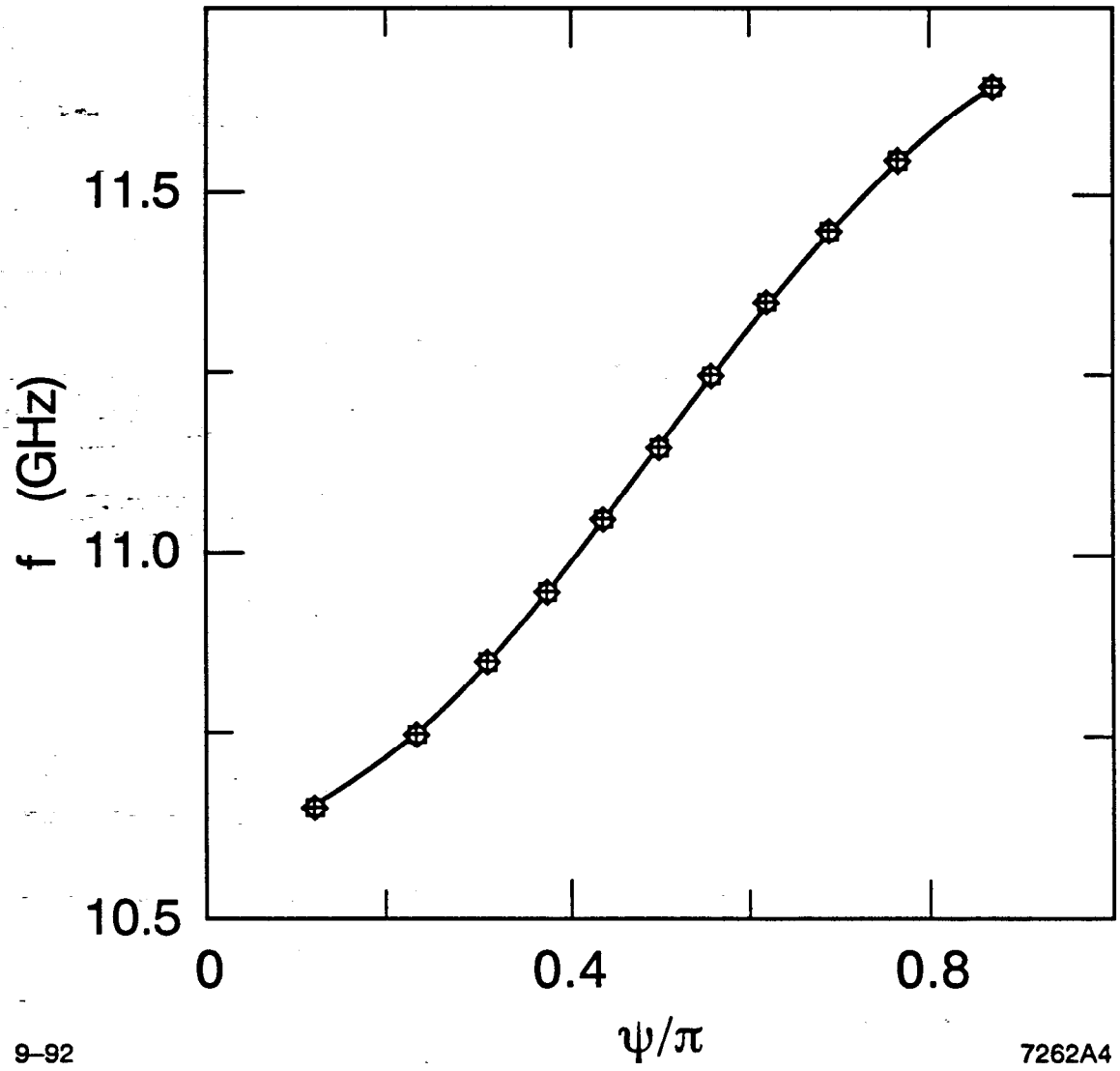

Fig. 4

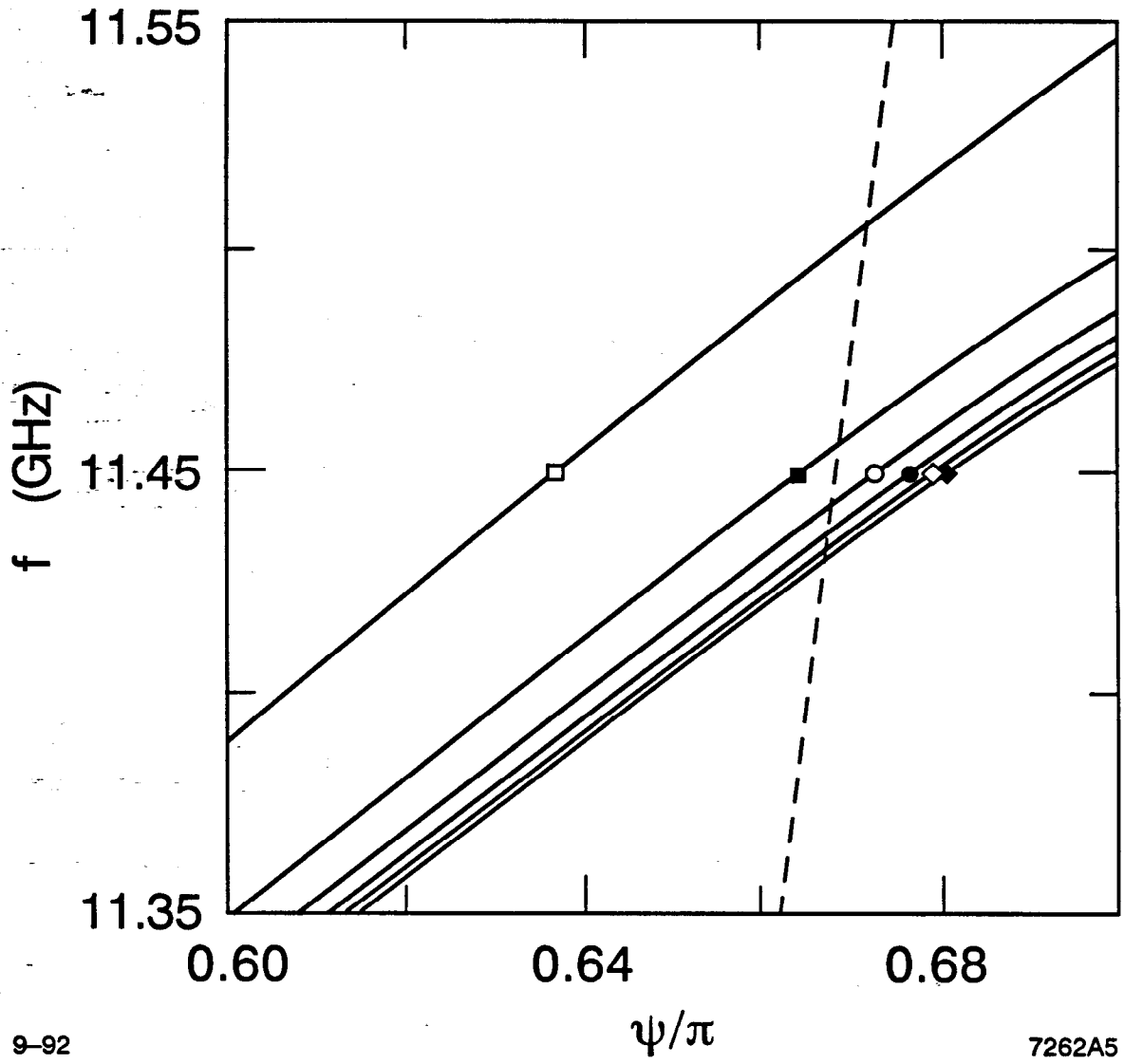

Fig. 5

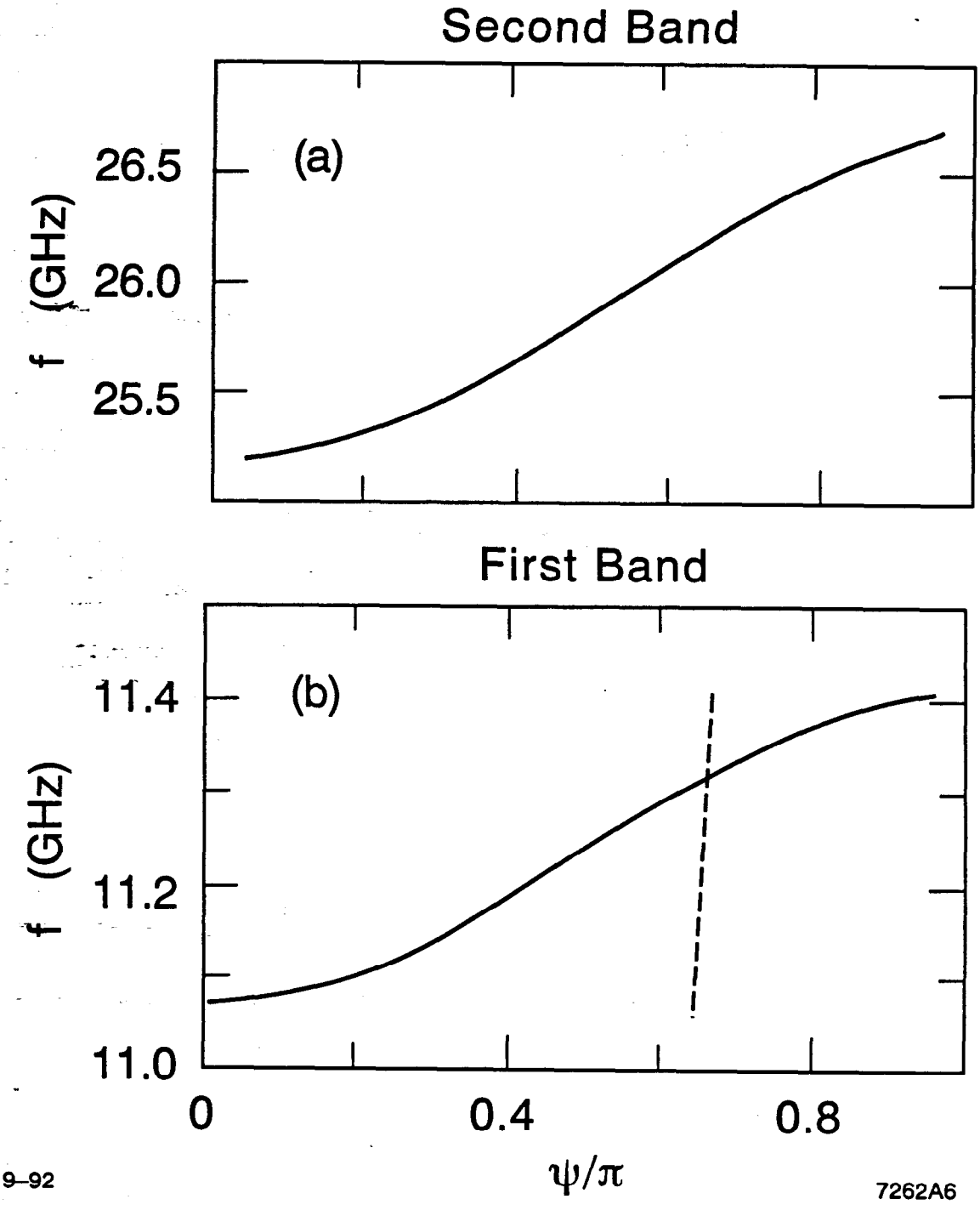
Second Band
(a)
26.5
26.0
25.5
f (GHz)
First Band
(b)
11.4
11.2
11.0
f (GHz)
0
0.4
0.8
ψ/π
9-92
7262A6

Fig. 6

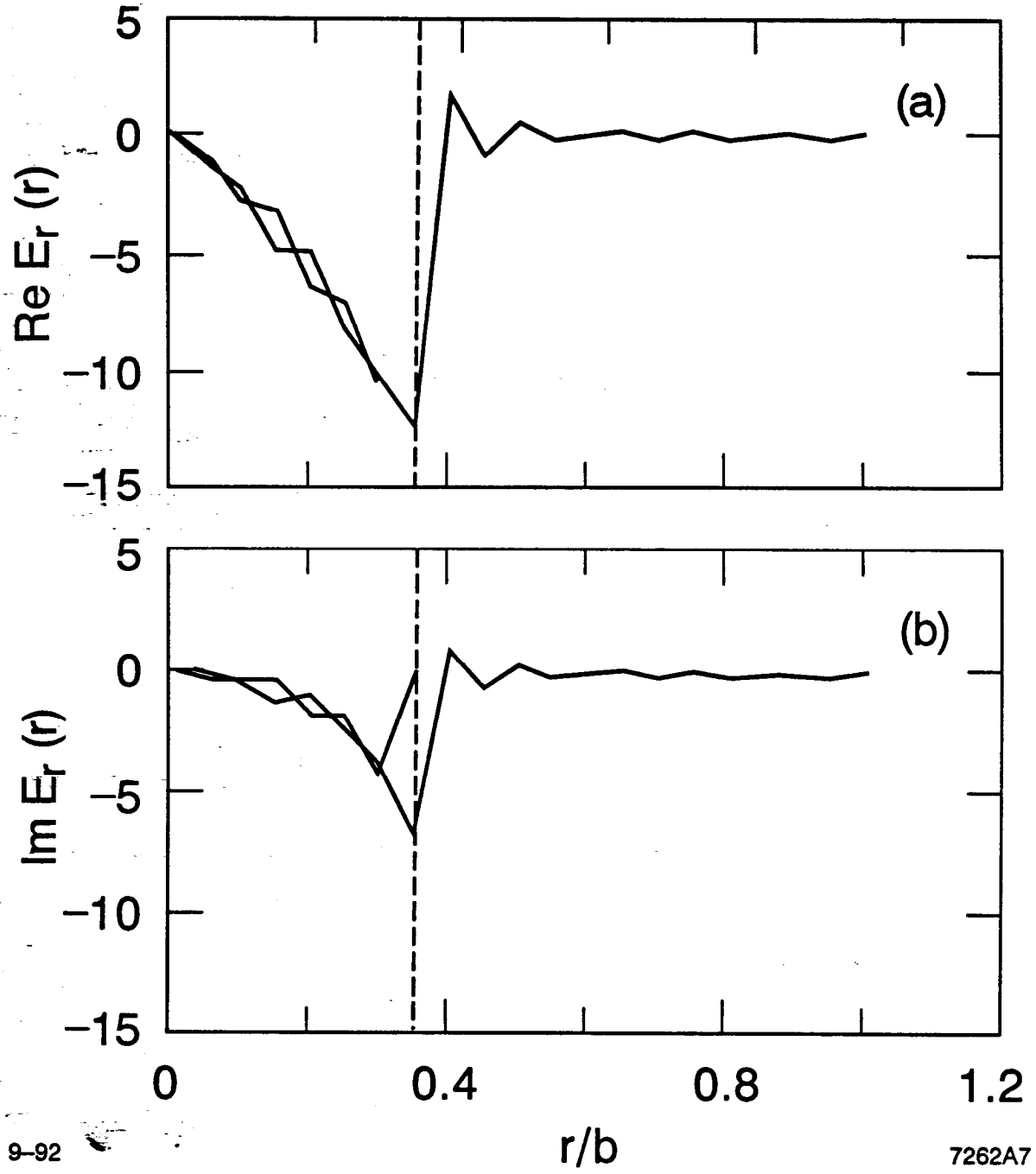

Fig. 7

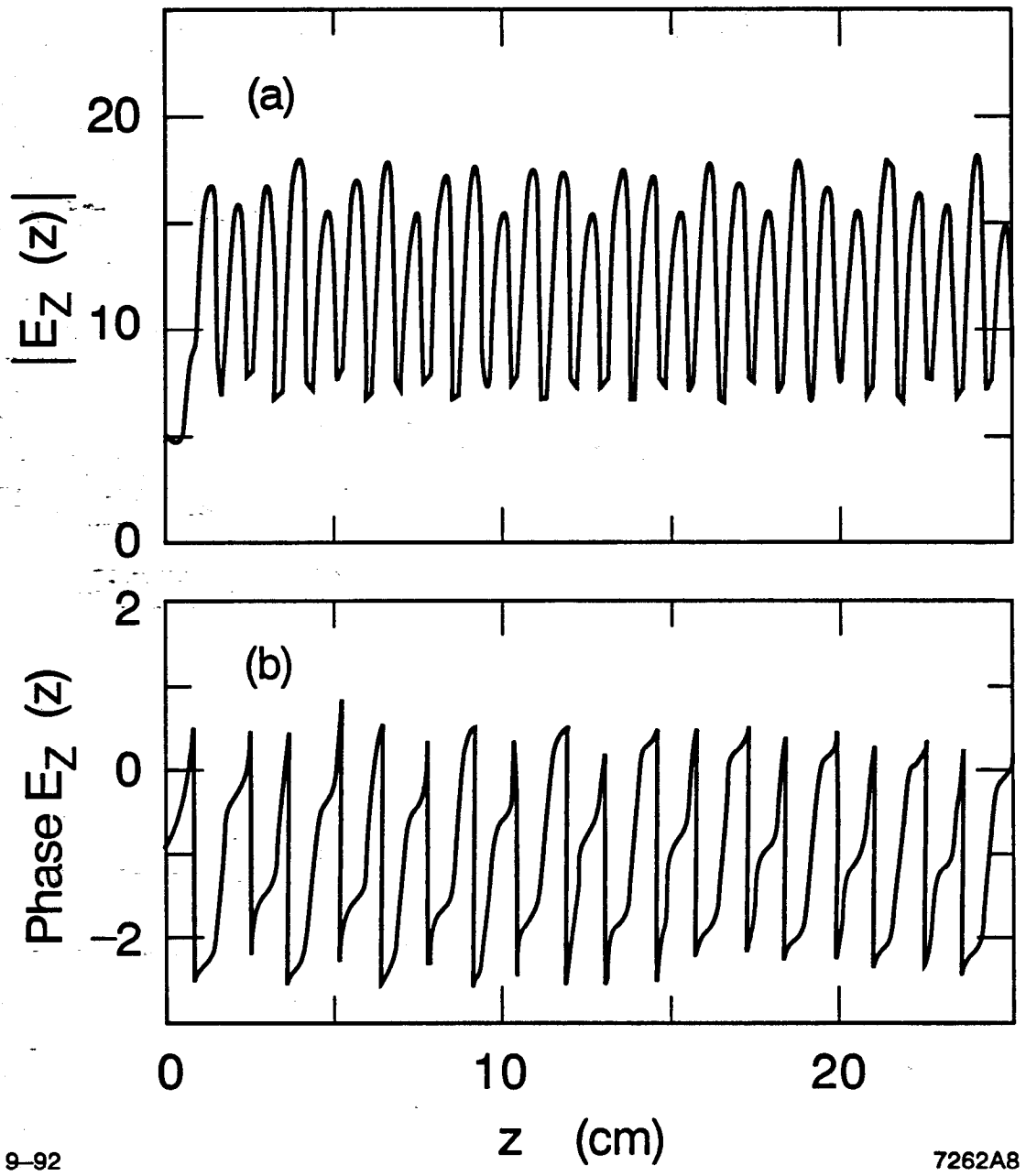

Fig. 8

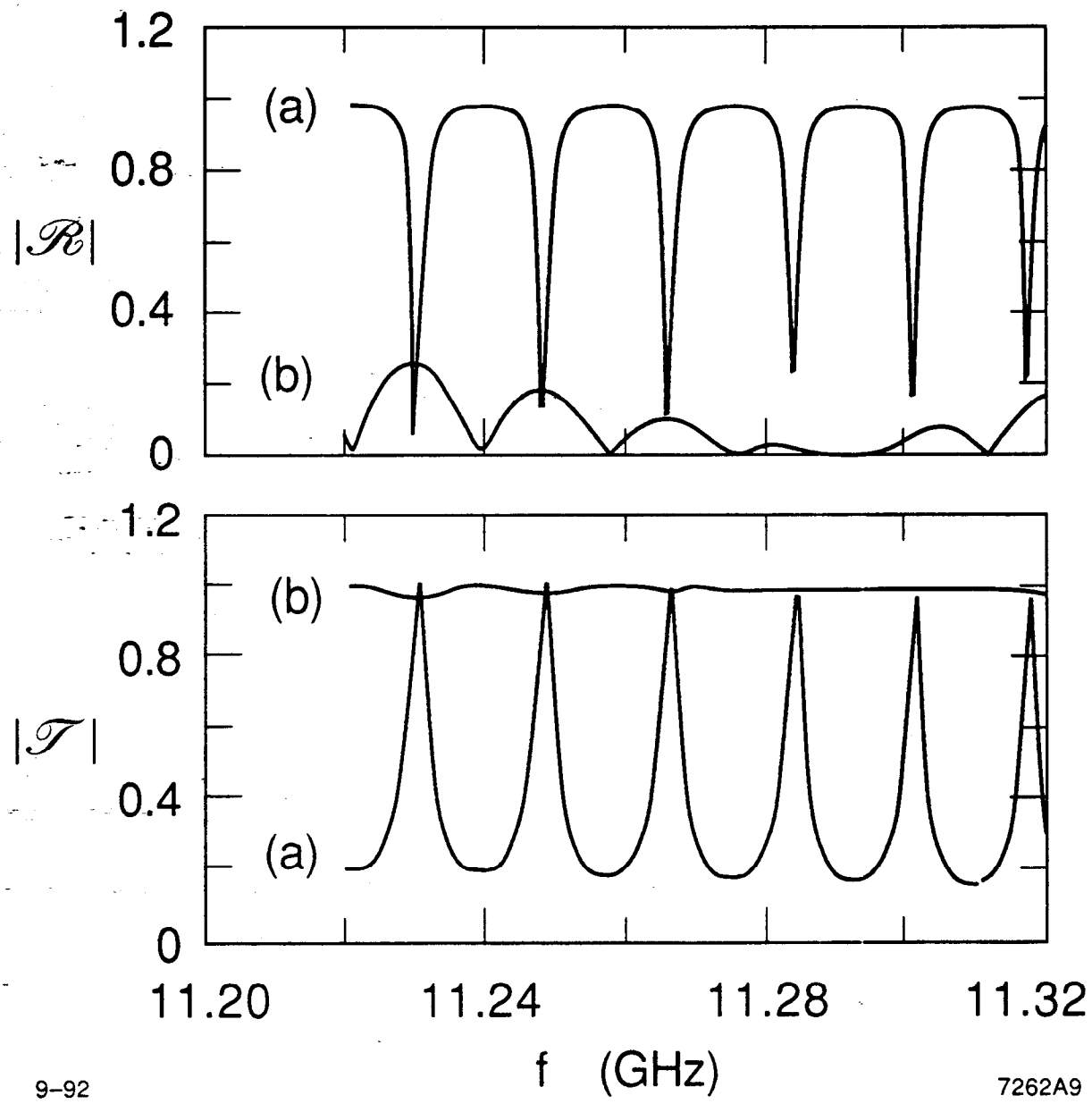

Fig. 9

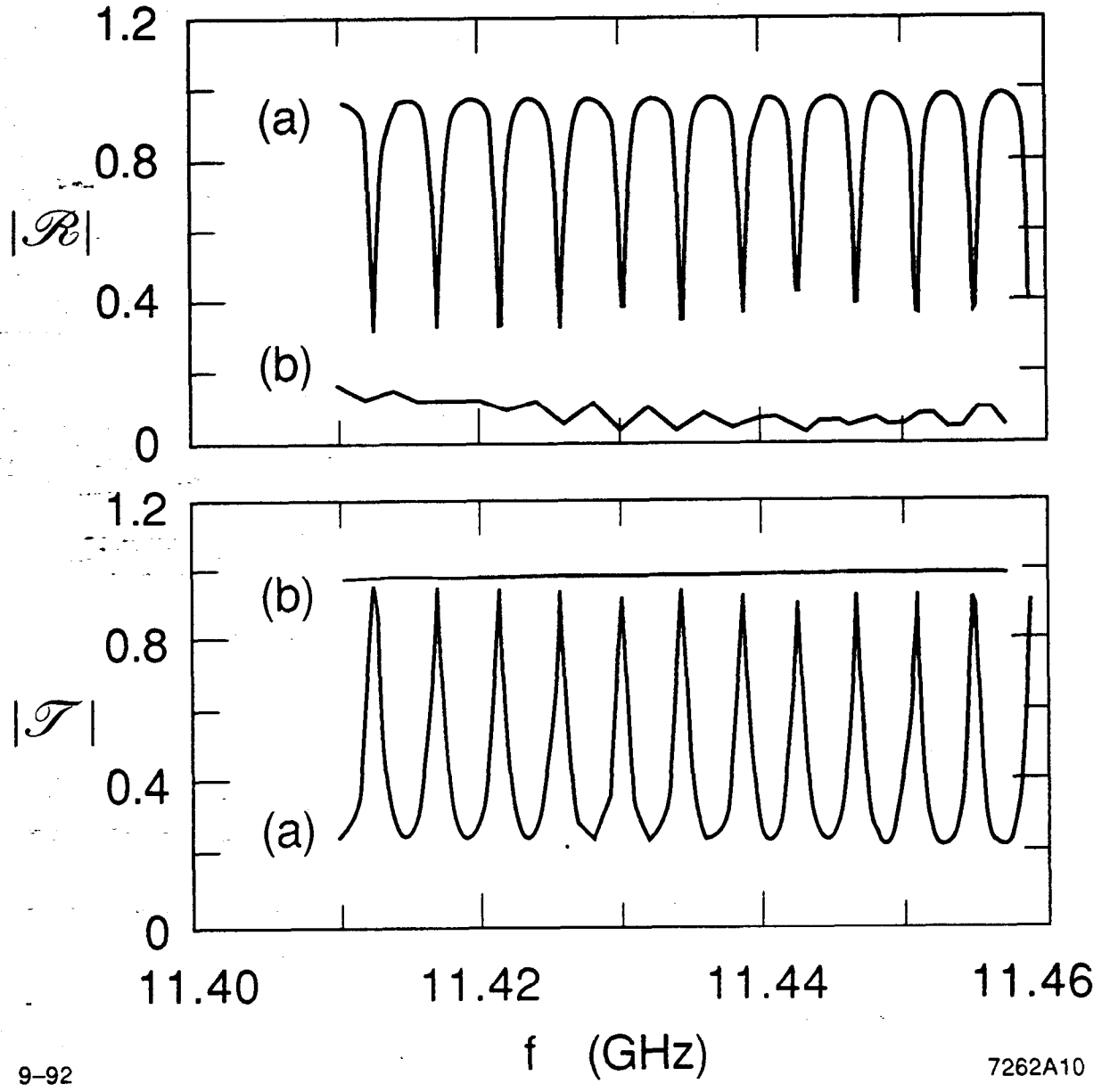
1.2
0.8
0.4
0
|ℛ|
(a)
(b)
1.2
0.8
0.4
0
|𝒯|
(b)
(a)
11.40
11.42
11.44
11.46
f (GHz)
9–92
7262A10

Fig. 10

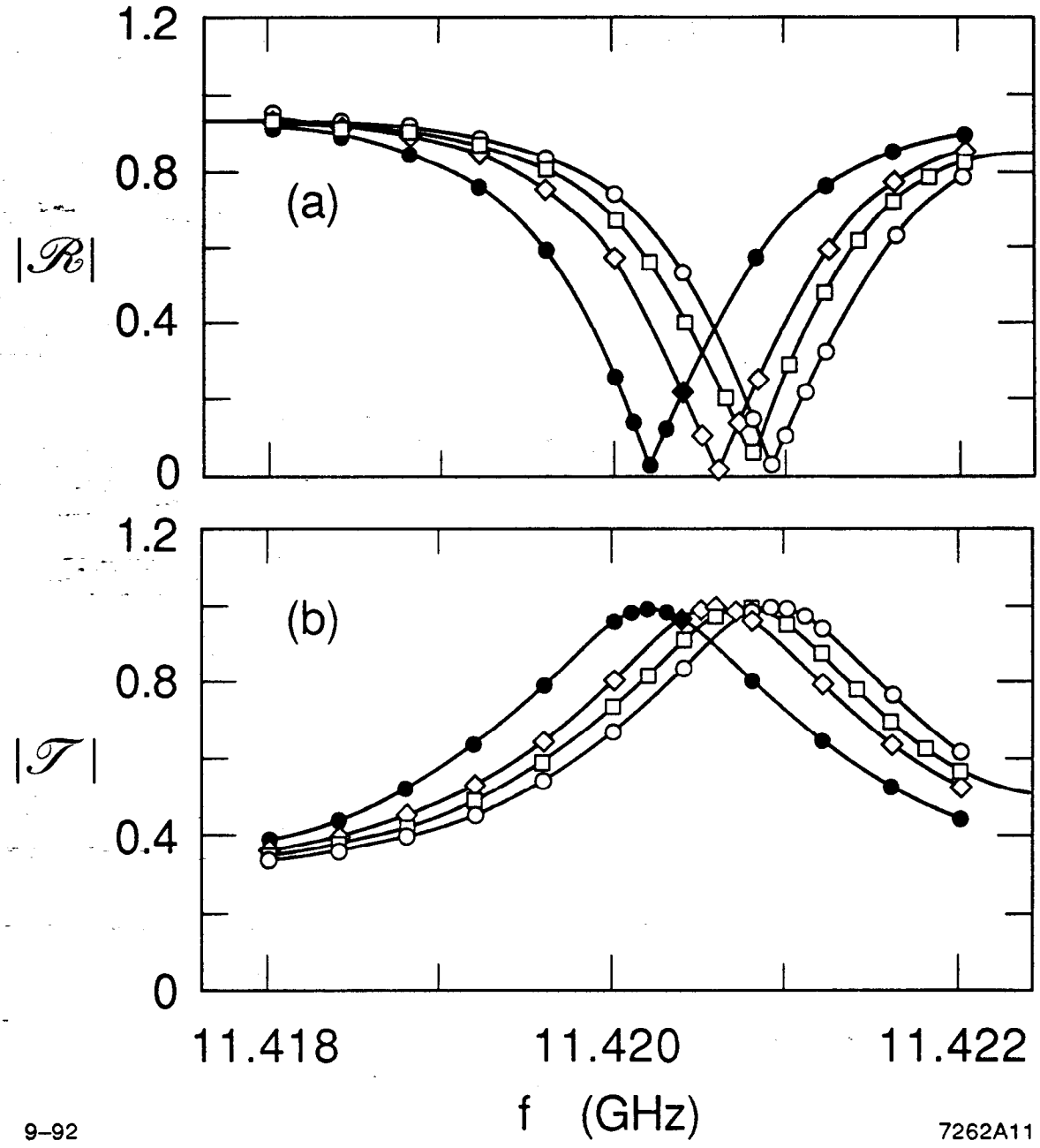

Fig. 11

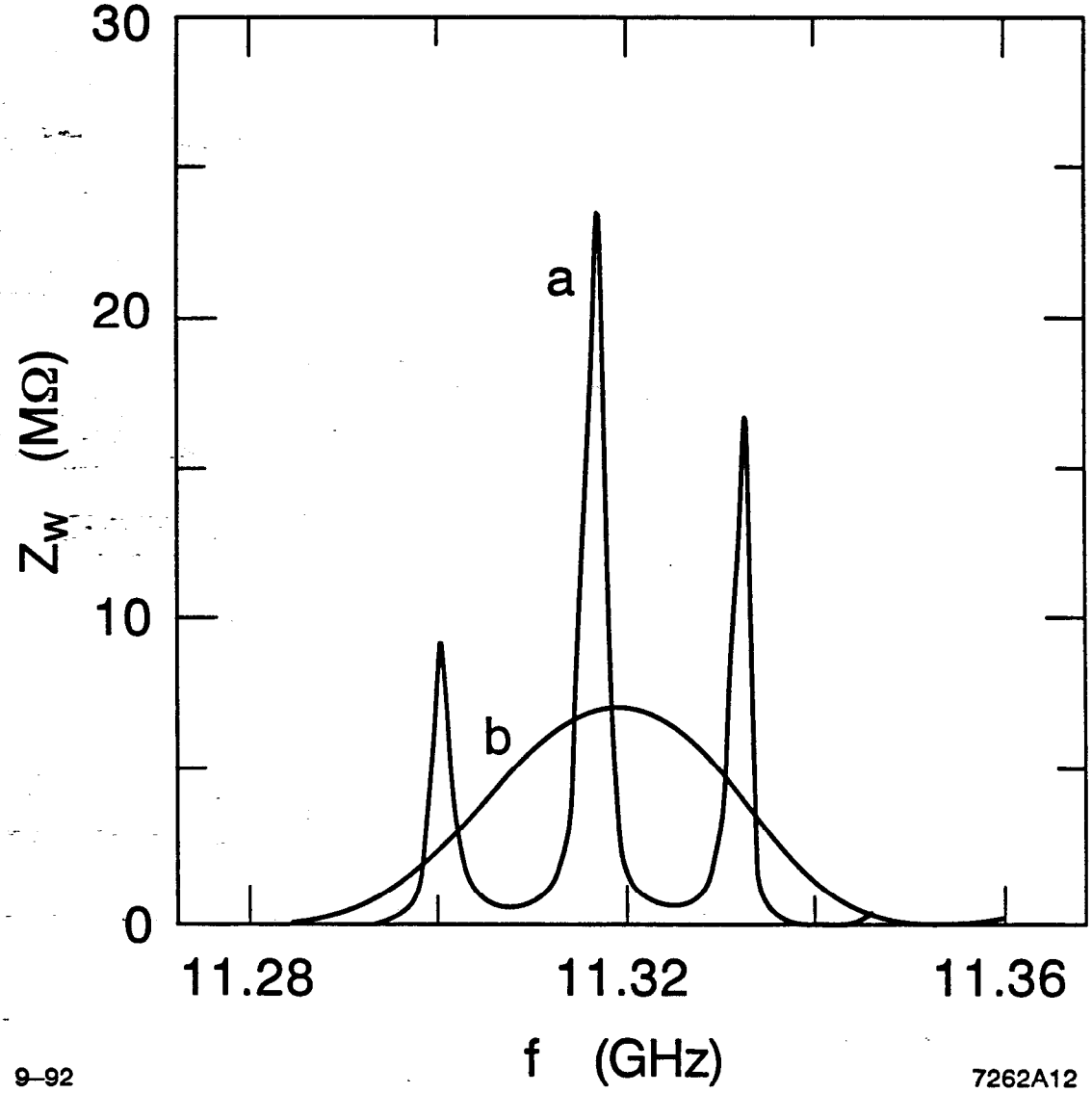

Fig. 12

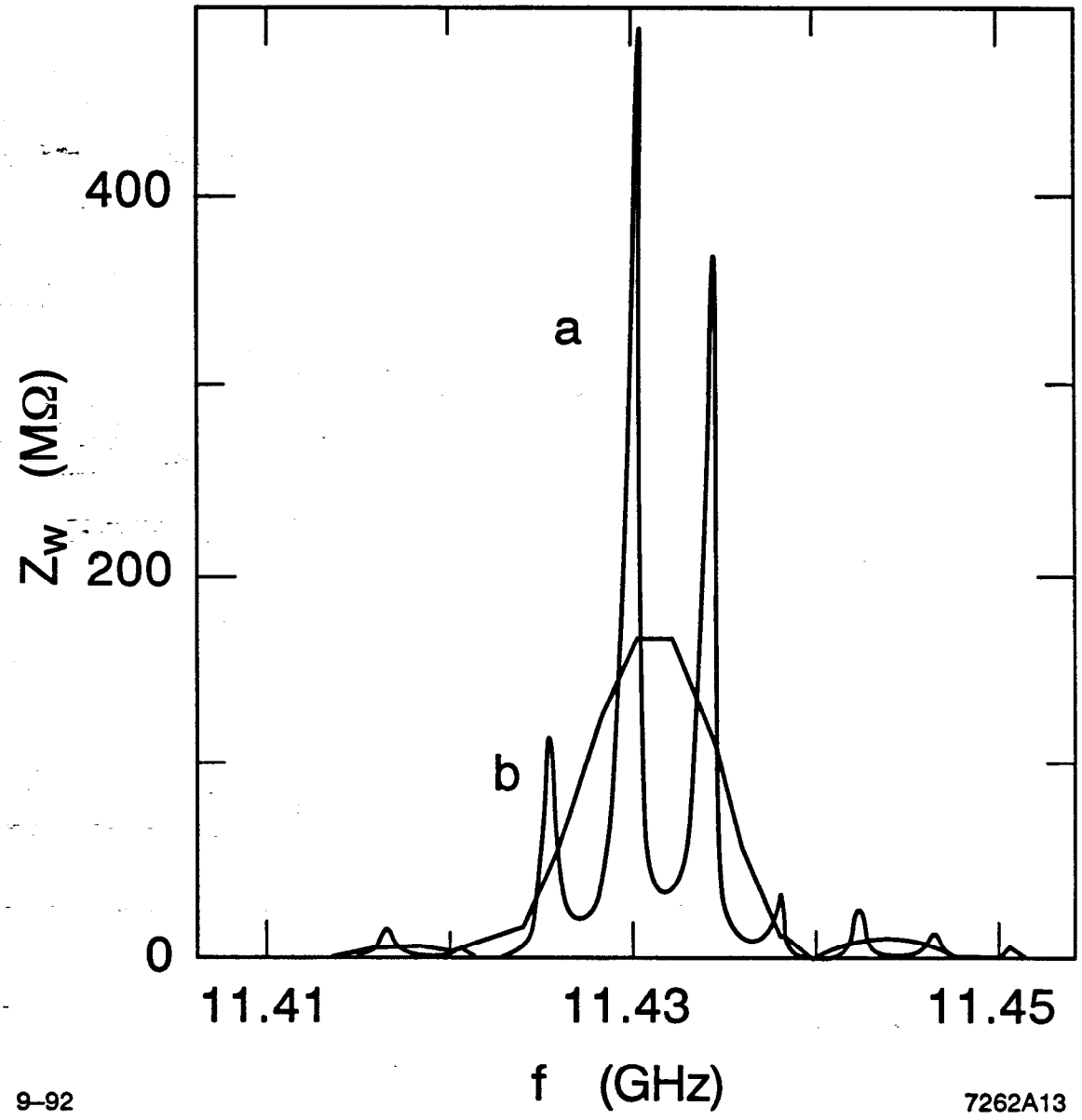

Fig. 13

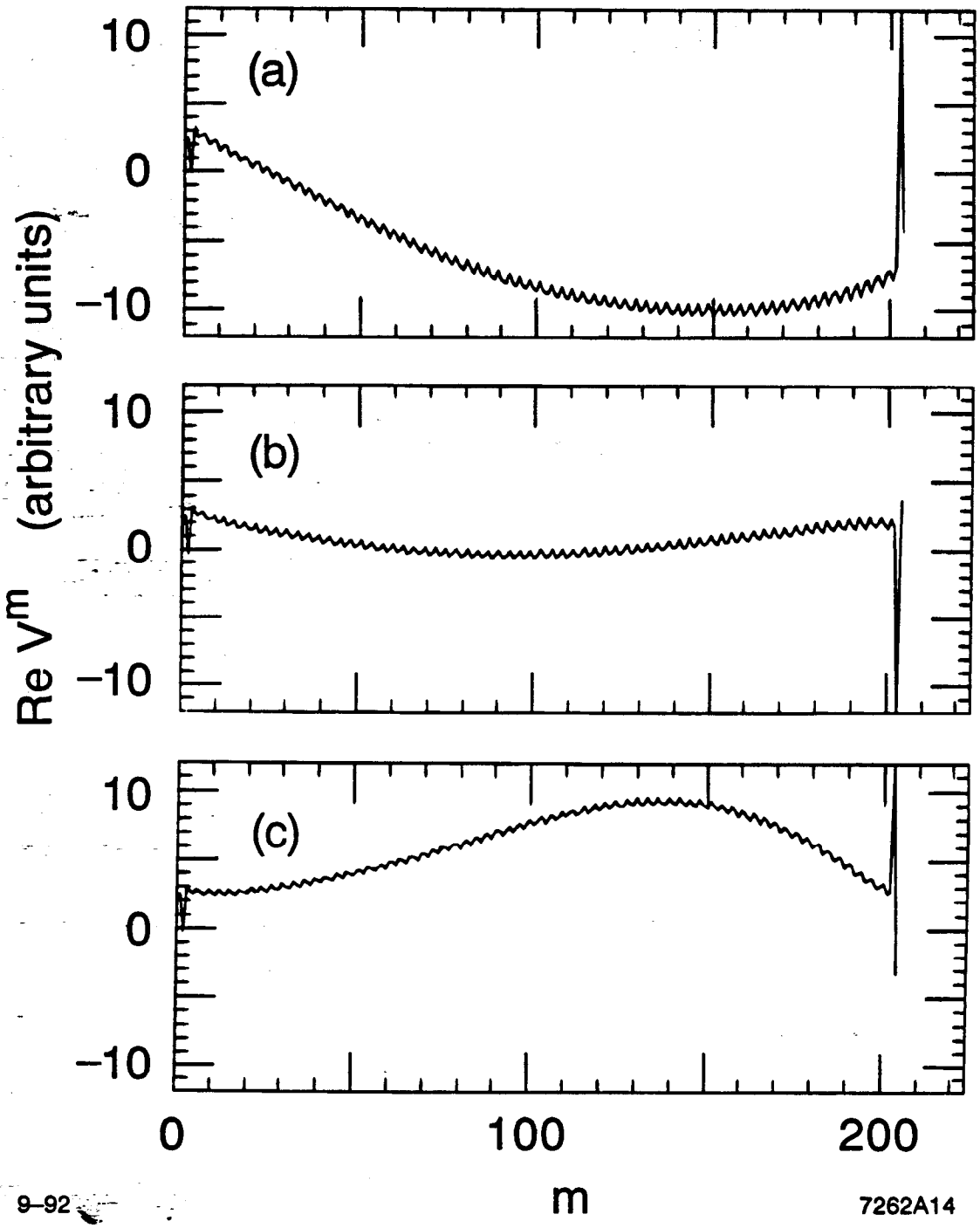
10
0
−10
(a)
10
0
−10
(b)
10
0
−10
(c)
Re V^m (arbitrary units)
0
100
200
m
9–92
7262A14

Fig. 14

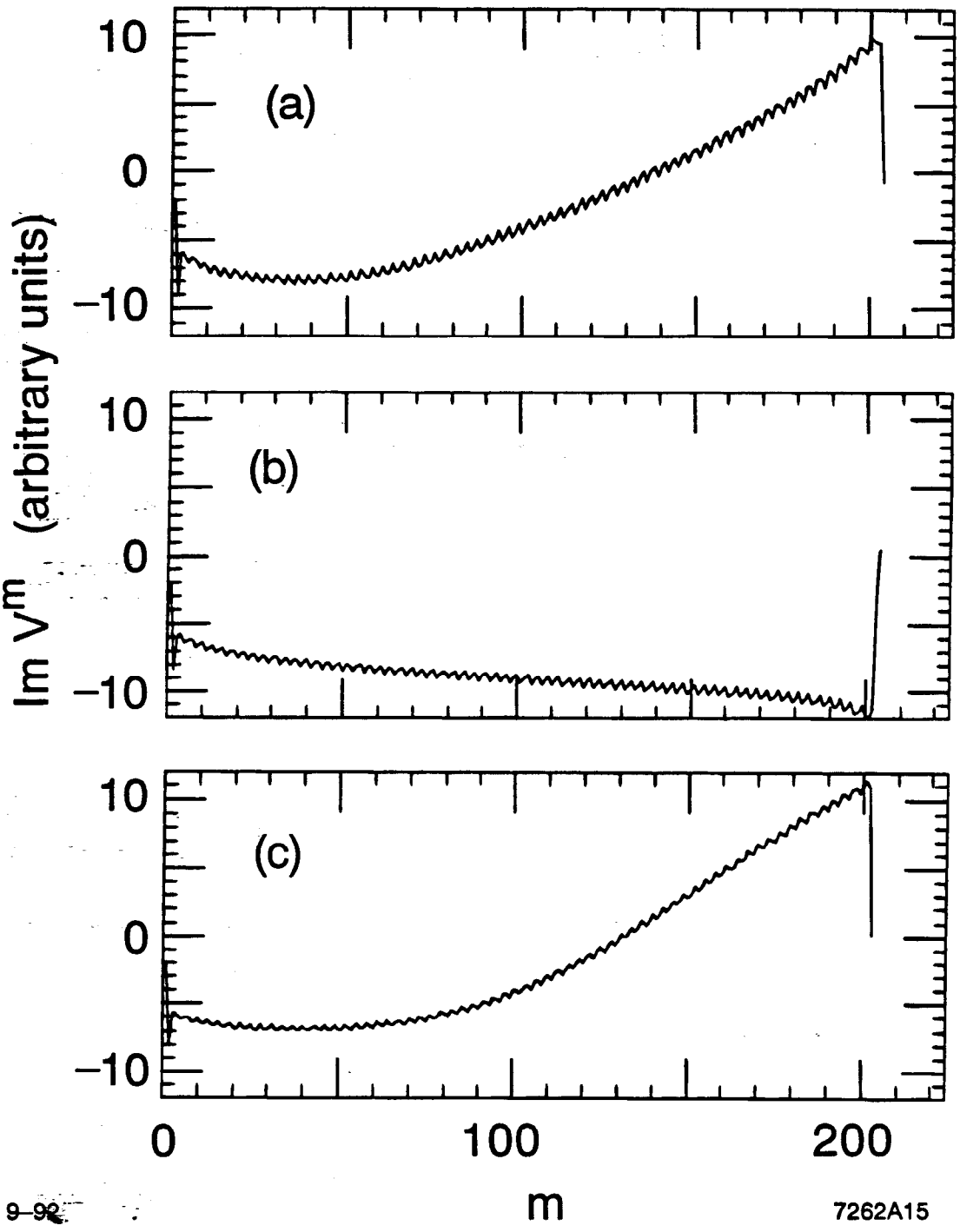
10
0
−10
(a)
10
0
−10
(b)
10
0
−10
(c)
Im V^m (arbitrary units)
0
100
200
m
9-92
7262A15

Fig. 15

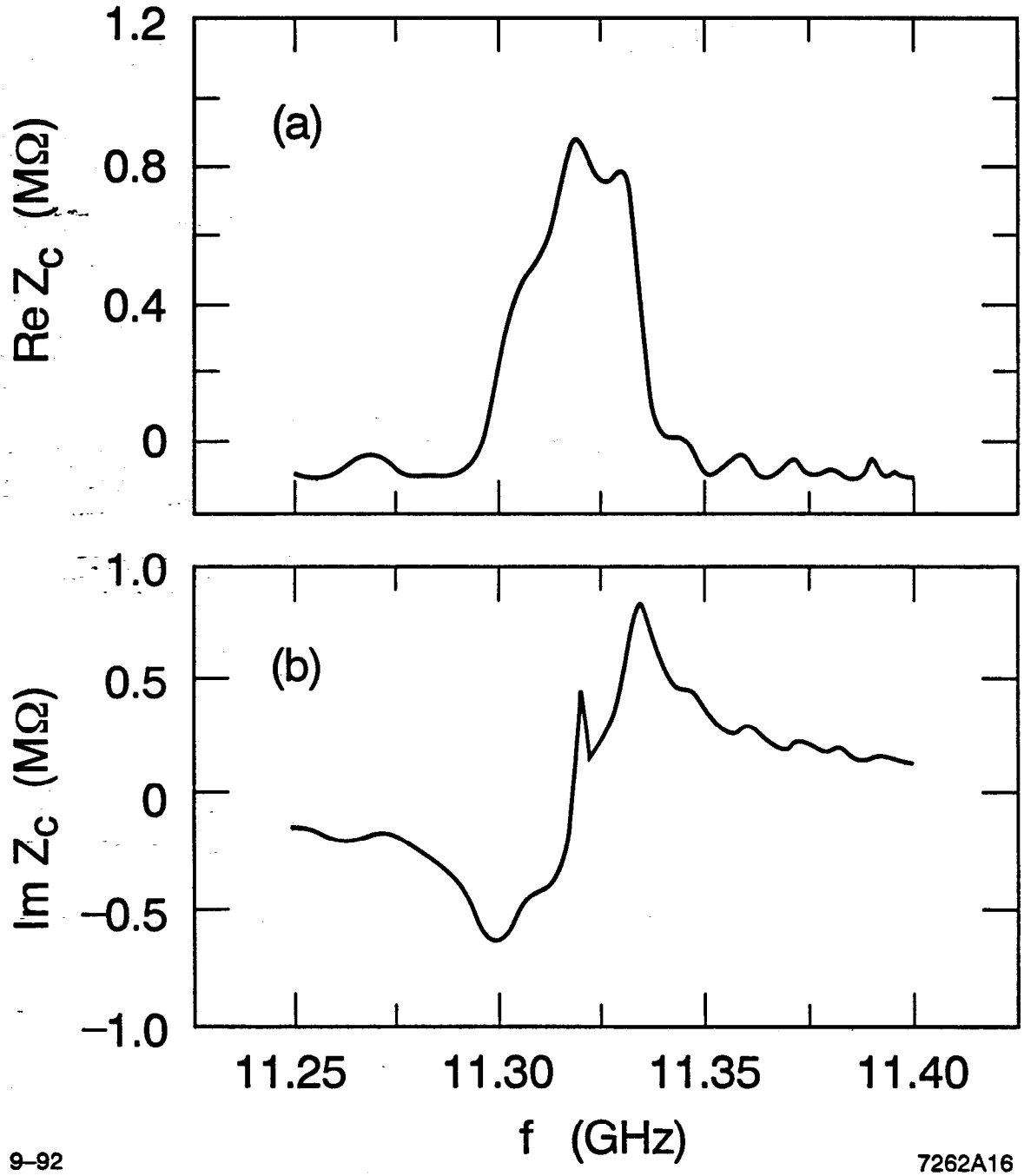
1.2
0.8
0.4
0
(a)
Re Z_c (MΩ)
1.0
0.5
0
−0.5
−1.0
(b)
Im Z_c (MΩ)
11.25
11.30
11.35
11.40
f (GHz)
9–92
7262A16

Fig. 16

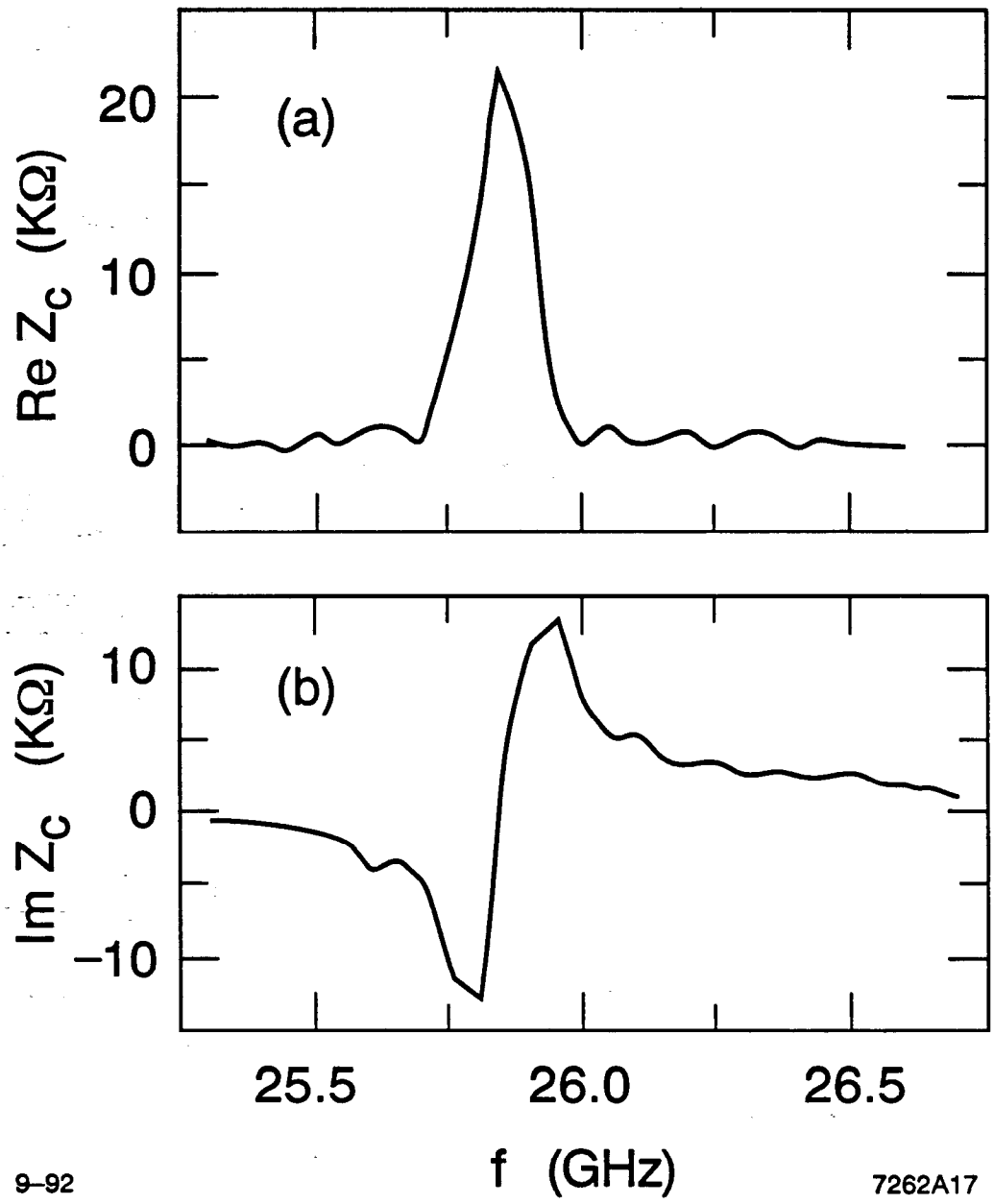

Fig. 17

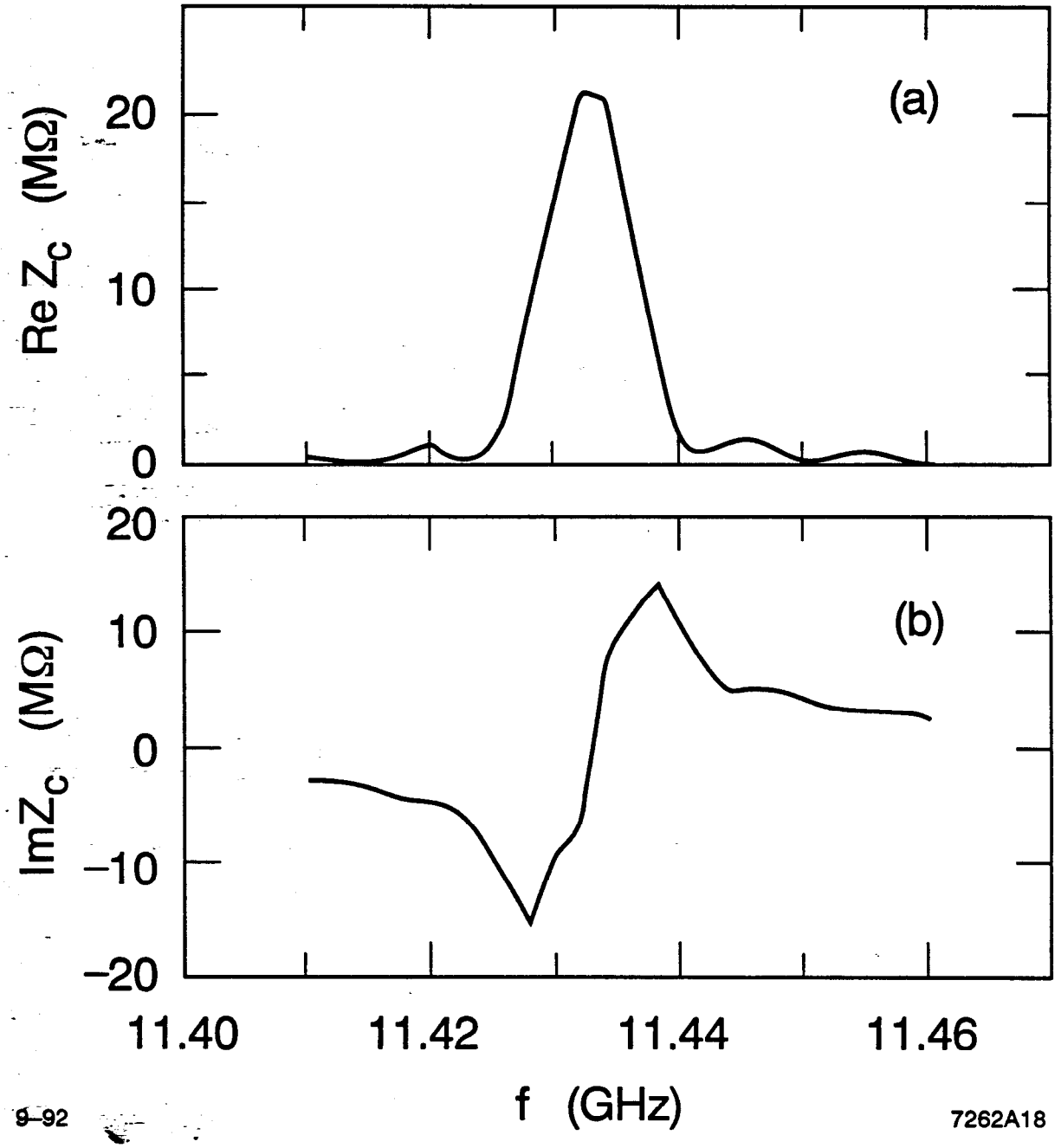
(a)
20
10
0
Re Z_c (MΩ)
(b)
20
10
0
−10
−20
ImZ_c (MΩ)
11.40
11.42
11.44
11.46
f (GHz)
9-92
7262A18

Fig. 18

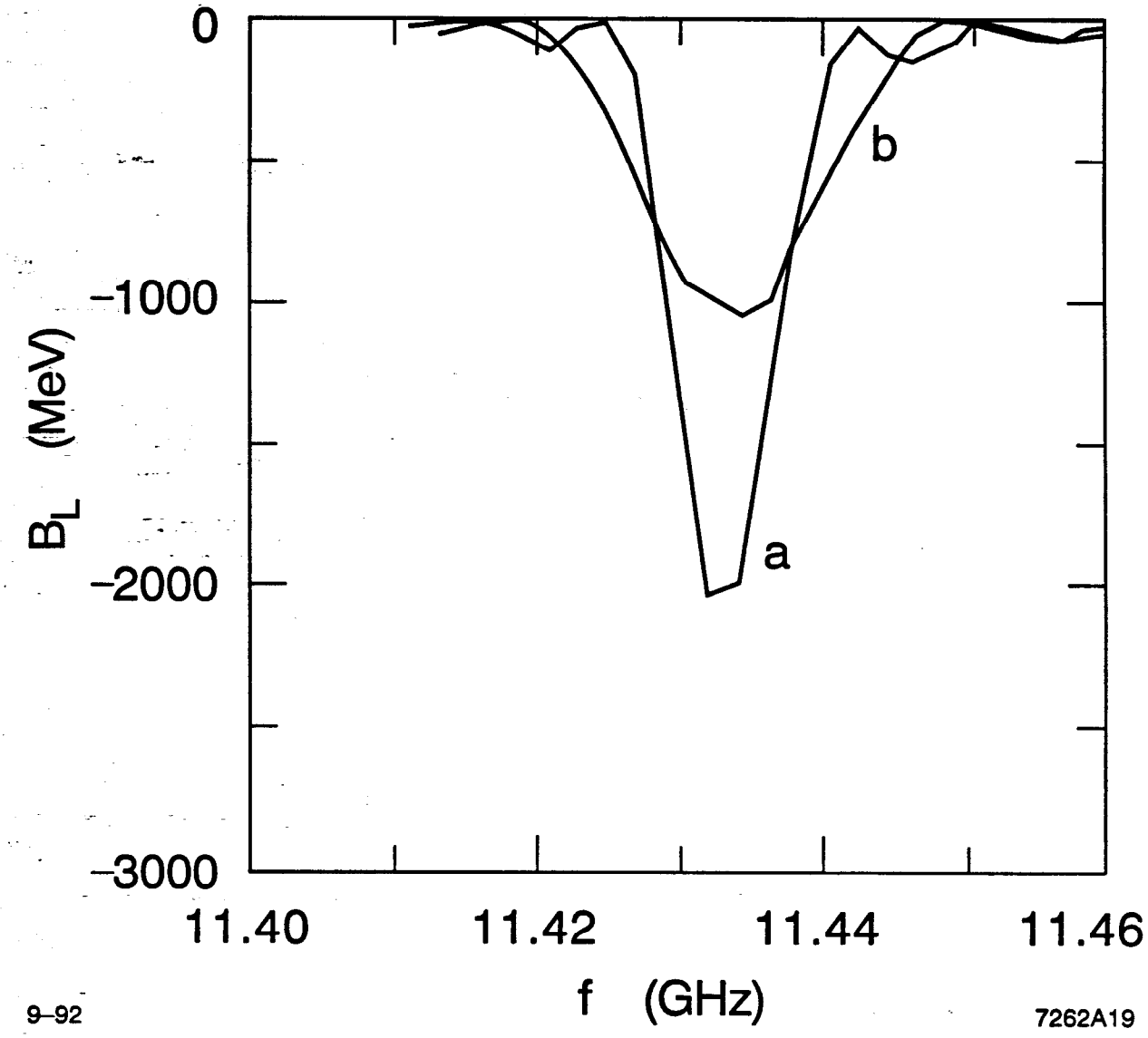
0
−1000
−2000
−3000
B_L (MeV)
11.40
11.42
11.44
11.46
f (GHz)
a
b
9–92
7262A19

Fig. 19

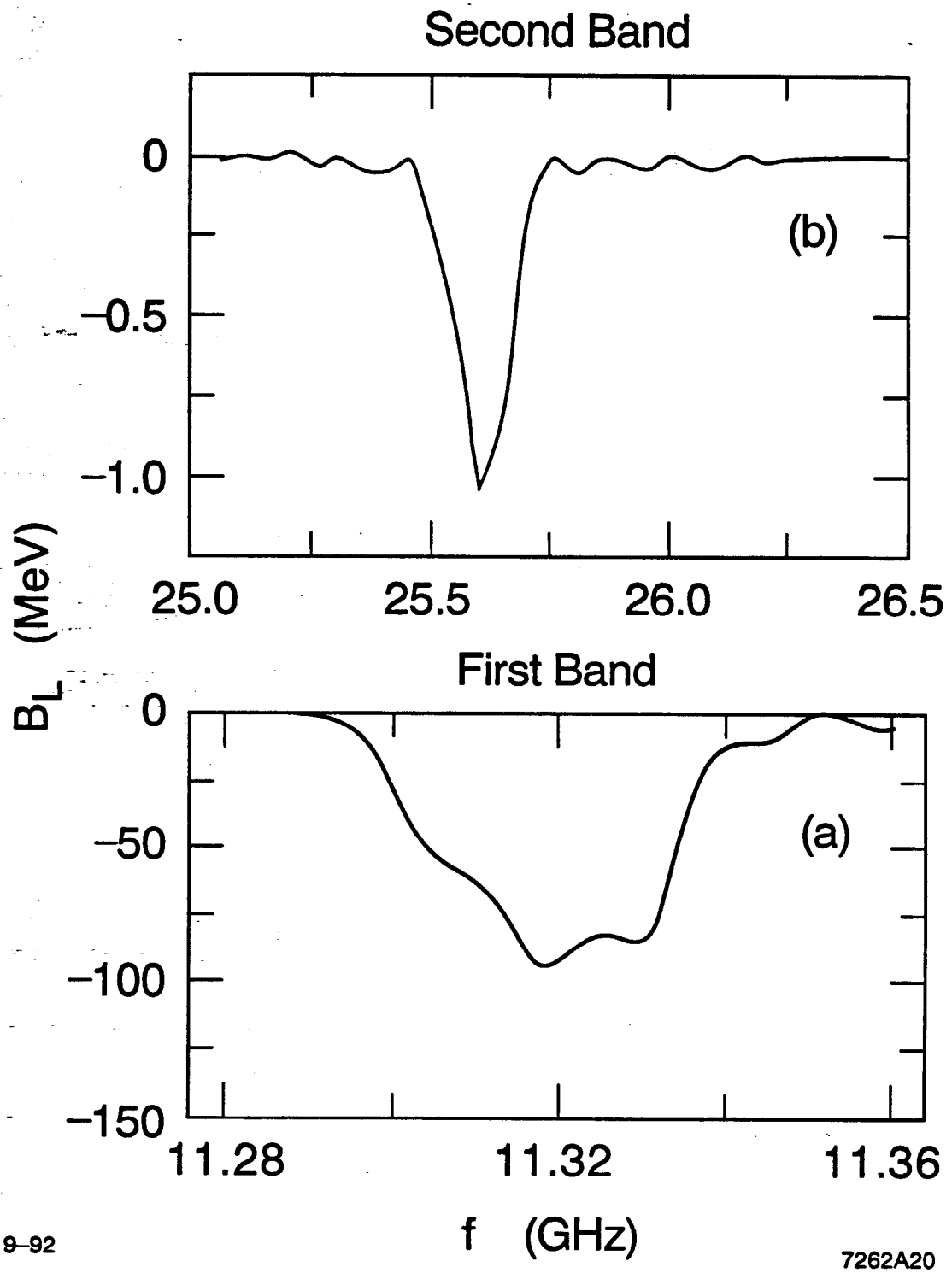
Second Band
0
−0.5
−1.0
(b)
25.0
25.5
26.0
26.5
First Band
B_L (MeV)
0
−50
−100
−150
(a)
11.28
11.32
11.36
f (GHz)
9–92
7262A20

Fig. 20